247 (2025) 213704

Contents lists available at ScienceDirect

Geoenergy Science and Engineering

journal homepage: www.sciencedirect.com/journal/geoenergy-science-and-engineering

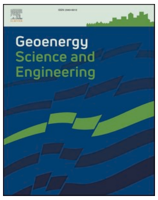

Hydrothermal fluid flow in Silurian carbonates in Lithuania and cold-water injection impact on long-term reservoir performance

Ieva Kaminskaite-Baranauskiene [a,b,*], Hakki Aydin [c], Zhida Liu [d]

[a] *Faculty of Chemistry and Geoscience, Vilnius University, Naugarduko st. 24, LT-03225, Vilnius, Lithuania*
[b] *GeoPower LT, Perkūnkiemio st. 19, LT-12120, Vilnius, Lithuania*
[c] *Zorlu Enerji, Manisa, Turkey*
[d] *National Key Laboratory of Continental Shale Oil, Northeast Petroleum University, Daqing, 163318, Heilongjiang, China*

ARTICLE INFO

Keywords:
Hydrothermal alteration
Pore evolution
CO_2-Water-rock interaction
PHREEQC
TOUGHREACT

ABSTRACT

The narrow barrier reef zone has been identified within the Silurian succession of the Baltic basin that stretches for hundreds of kilometres in a north-south orientation across central Lithuania. The reefs have been widely explored by drilling due to accumulations of oil. Even though the oil production proved economically unfeasible, infrastructure of over 70 wells is left behind that could be reused for geothermal purposes. In this study, hydrothermal fluid flow products were examined across the Silurian column to identify natural deformation mechanisms affecting petrophysical properties of the rocks. The cores showing hydrothermal alteration have been analysed by macro- and microscopic petrography, cathodoluminescence and SEM microscopy, XRD, C and O stable isotope and liquid-vapour inclusion analyses. Then, thermo-chemical numerical models were run of cold-water injection and low enthalpy geothermal energy extraction from the reef reservoirs within the Silurian section. CO_2-water-rock interaction simulations were performed for three different cases to capture different rock and formation water types observed in the wells, including 1) calcite-rich reef interval within the largest Kudirka structure; 2) dolomitized Kudirka reef interval; and 3) interval within the Pavasaris structure in the central part of the barrier reef zone. The results show that during a cold-water injection, a decline in temperature coincided with a decrease in pH. This combined effect resulted in the dissolution of dolomite and calcite minerals, evident from the observed decrease in their volume fraction and the corresponding rise in the concentration of Ca^{2+} and Mg^{2+} ions. This had a positive effect on porosity. Petrographic analysis of Silurian carbonate rocks and manifestations of hydrothermal processes within them also indicate that porosity of the rocks was maintained through several stages of dissolution. Hydrothermal alteration products as well as oil stains were found within the vugs, solution-enlarged fractures, stylolitic surfaces as well as tension-gashes associated to stylolites, suggesting that they acted as conduits to fluid flow. The largest porosity losses of the Silurian reefs are associated with the two largest thermal events that have taken place during the Late Silurian-Devonian continent-continent collision as well as the Carboniferous-Permian rifting and magmatism, that provided external heat sources (temperatures reaching 70–140 °C) creating suitable conditions for cementation. Therefore, low temperatures of the reservoirs and cold-water injection may act in advantage to sustainable water production.

1. Introduction

In the context of the Energy Transition, the significance of natural resources like geothermal energy is escalating. The shift from hydrocarbon-based to sustainable energy sources is a critical research focus. Enhancing well performance and preventing reservoir clogging during production and injection are key challenges in geothermal reservoir engineering. The drawdown of the groundwater table during exploitation limits the long-term, sustainable use of convection-type resources, making reinjection essential. Injecting cold wastewater into a reservoir can lower reservoir temperature and, depending on pressure, cause CO_2 to dissolve or degas into the water. Fluid injection may also positively alter pore pressure, reducing the effective stress on the reservoir rock (Biot, 1956). Consequently, changes in the chemical composition, redox conditions, and temperature of reinjection water can trigger CO_2-water-rock interactions, impacting reservoir porosity and

---

* Corresponding author. Faculty of Chemistry and Geoscience, Vilnius University, Naugarduko st. 24, LT-03225, Vilnius, Lithuania.
E-mail address: ieva.kaminskaite888@gmail.com (I. Kaminskaite-Baranauskiene).

https://doi.org/10.1016/j.geoen.2025.213704
Received 30 July 2024; Received in revised form 16 January 2025; Accepted 17 January 2025

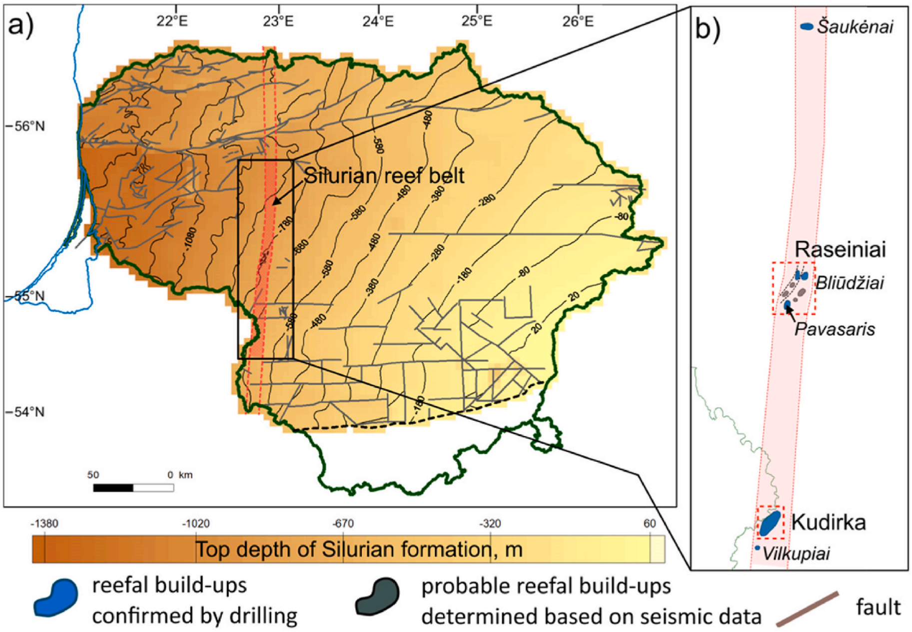

Fig. 1. a) Structural map of the top depth (m) of the Silurian succession; and b) a zoomed in map illustrating the studied reef structures within the Silurian reef belt (after Micklethwaite and Cox, 2004; Kaminskaite-Baranauskiene et al., 2024). Study areas for simulation analysis are marked with dashed red contours. (For interpretation of the references to colour in this figure legend, the reader is referred to the Web version of this article.)

Table 1
Rock properties of the reef intervals used for modelling. Porosity-permeability measurements were done on the core samples taken from the wells (the data was taken from the well end reports).

	Calcite-rich Kudirka	Dolomitized Kudirka	Pavasaris Reef
Thickness, m	88	88	45
Effective Thickness, m	23	23	19
Porosity, %	8.9	11	7.9
Permeability, mD	2.7	10	8

Table 2
Rock composition of the reef intervals determined by the XRD analysis used for water-rock interaction modelling.

	Calcite-rich Kudirka	Dolomitized Kudirka	Pavasaris Reef
Calcite, %	86.49	2.51	92.20
Dolomite, %	2.85	85.35	0.93
Quartz, %	3.23	2.09	0.22
Pyrite, %	0.15	0.68	3.63
Anhydrite, %	5.60	1.64	5.86
Illite, %	1.32	1.30	0.11

permeability (e.g., Su et al., 2018; Hou et al., 2022; Cheng et al., 2024).

When external brine is injected into a reservoir, the rock-fluid system seeks to re-establish equilibrium by dissolving primary minerals and precipitating secondary minerals in the reservoir rock. The mineralogical composition of the rock and the solubility of its constituent minerals dictate the sequence in which minerals dissolve and precipitate. Supersaturation within the fluid induces mineral precipitation. In a closed system, calcite solubility increases with decreasing temperature, and dissolution by water or aggressive fluids saturated with acids or CO_2 may create high permeability zones (Schmoker and Halley, 1982; Palmer, 1991; Andre and Rajaram, 2005). Therefore, the injection of cold CO_2-rich wastewater into a reservoir results in calcite undersaturation, preventing the precipitation of carbonate minerals around the injection well, whereas dissolution will further widen fracture apertures, enlarge pores and create vugs (Sigfússon and Uihlein, 2015). However, dissolved calcite can migrate and precipitate as cement in adjacent rock, making the reservoir regionally and locally heterogeneous due varying amounts of cement and karstification (Garrison, 1981).

The introduction of air into reservoirs, often due to inadequate sealing of reinjection wells or another onland infrastructure, can increase dissolved oxygen levels, triggering redox reactions. In reservoirs containing pyrite, this can lead to the dissolution of iron (Fe) and the subsequent precipitation of minerals such as $Fe(OH)_3$, goethite, and siderite, which alters the ionic composition and pH of the water (Su et al., 2018). Additionally, high sulphate concentrations may

Table 3
USGS for activation energy and kinetic rate constant of minerals used for modelling (from Palandri and Kharaka, 2004).

	Activation Energy (kj/mol)	Kinetic rate (mol/mol^2/s)
Calcite, %	23.5	1.023×10^{-9}
Dolomite, %	52	2.95×10^{-8}
Quartzite, %	87	1.023×10^{-14}
Pyrite, %	56	2.8×10^{-5}
Anhydrite, %	73	1.0×10^{-4}
Illite, %	19.6	3.0×10^{-13}

Table 4
Aqueous complexes used for modelling with TOUGHREACT.

$Ca(HCO_3)+$	$CaCO_3$ (aq)	$CaCl+$	$H2SiO_4^{-2}$
$CaCl_2$ (aq)	$CaOH^+$	$CaSO_4$	$Mg(HCO_3)^+$
$MgCO_3$ (aq)	$MgCl^+$	MgF^+	$MgSO_4$
NaBr (aq)	NaF (aq)	$NaHCO_3$	$NaSO_4^-$
OH^-			

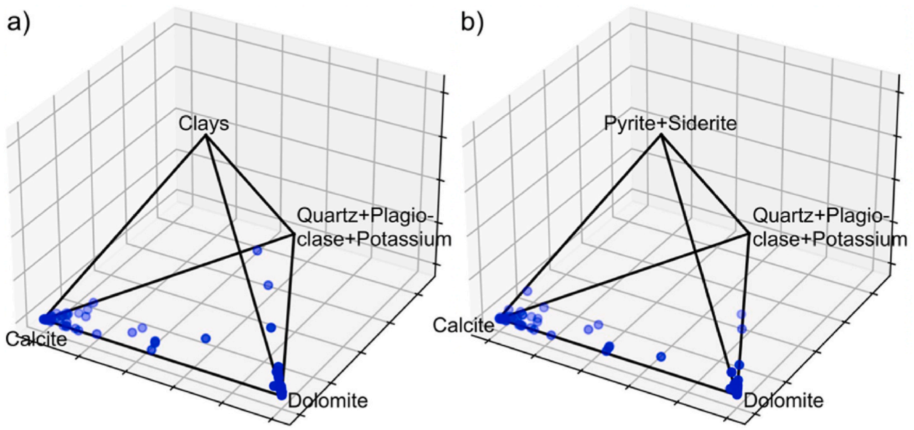

Fig. 2. 4D ternary plots of XRD results representing compositions including calcite, dolomite, quartz together with plagioclase and potassium feldspar, as well as a) clays, and b) pyrite with siderite.

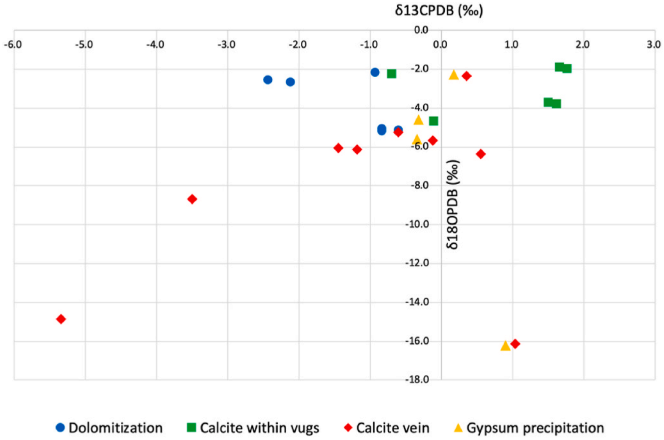

Fig. 3. $\delta^{13}C$ and $\delta^{18}O$ data of the hydrothermal products collected from the wells penetrating the Silurian carbonate formation in Lithuania.

accumulate in the discharge zones, stemming from the oxidation of sulphide minerals like pyrite, the dissolution of gypsum and anhydrite, or the transformation of hydrogen sulphide-rich deep fluids into sulphuric acid upon contact with oxygenated water (Goldscheider et al., 2010). The authors indicate a direct correlation between sulphate levels and temperature, and an inverse correlation with discharge.

Carbonate minerals exhibit high reactivity, leading to significant porosity reduction through hydrothermal recrystallization and cementation. However, tectonic deformations and associated hydrothermal processes, such as dissolution, dolomitization, silicification, and thermochemical sulphate reduction, often contribute to the formation of effective reservoirs at greater depths (Zhu et al., 2010; Jiang et al., 2015; Biehl et al., 2016; Jiang et al., 2017; Menezes et al., 2019; Jiu et al., 2020, Li et al., 2022, 2023). The sustainable fluid flow is crucial for geothermal energy production. Therefore, understanding the processes underlying scaling and its prevention under natural conditions is essential for developing strategies to ensure long-term energy production. The chemical composition of geothermal water is a critical factor in planning geothermal systems, as it can influence installations through corrosion, scaling or reservoir clogging (Wagner et al., 2005).

Hydrothermal alterations of reservoir rock serve as indicators of the nature and temperature of the groundwater fluids that circulate within the rock, also revealing their temporal and spatial extent within the reservoir (Ledésert et al., 2010). Therefore, in this work, natural hydrothermal systems are studied within Silurian carbonate rocks in Lithuania including: 1) formation water composition, 2) rock content, and 3) natural hydrothermal alterations of the rocks within these systems. Pore evolution and hence fluid flow conduit system sustainability is evaluated for the lifetime of the Silurian carbonate formations.

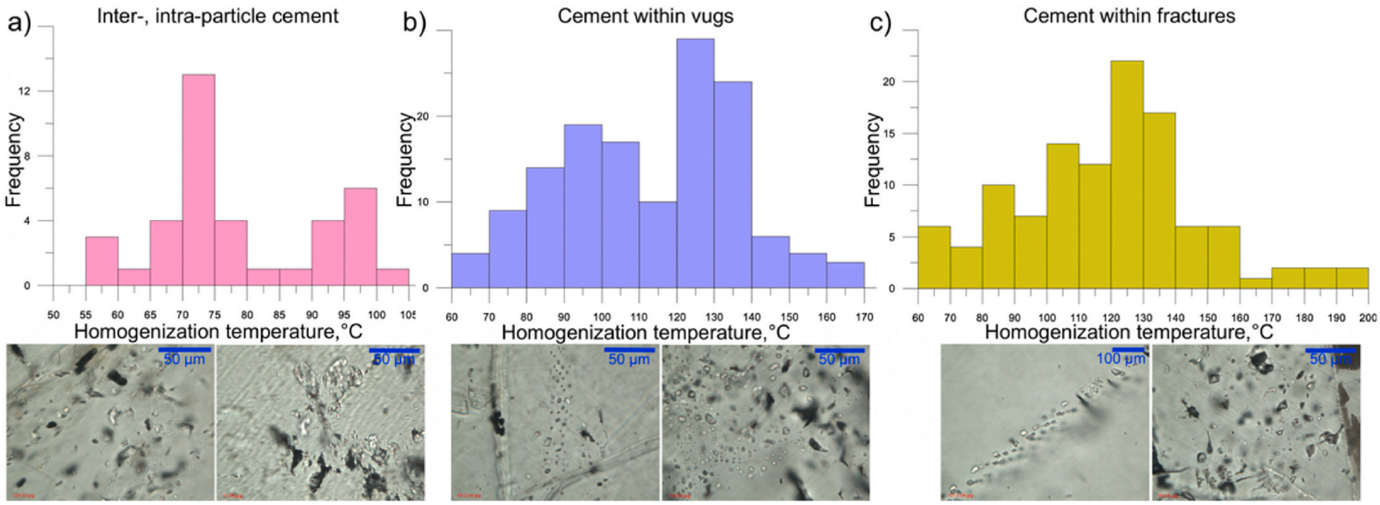

Fig. 4. Homogenization temperature histograms of inclusions found within: a) inter-, intra-particle calcite cement; b) sparry calcite cement within vugs; and c) veins. Below are the images of the analysed two-phase liquid-vapour inclusions for each group.

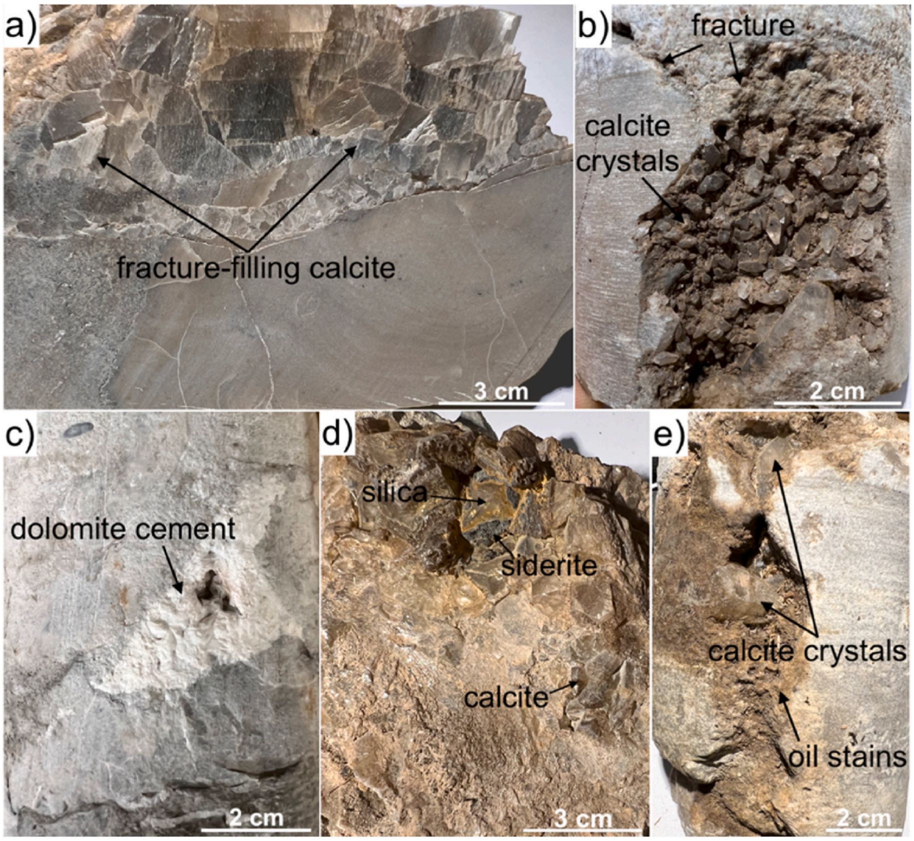

Fig. 5. Core photos showing cementation within Silurian carbonate succession in Lithuania: a) calcite cement partially filling fracture/vein with aperture of up to 8 cm within stromatoporoid limestone (Bliūdžiai-156 well, 947.8 m depth); b) calcite crystals encrusting fracture surface, note the open fracture perpendicular to the encrusted fracture showing dissolution enlarged vuggy surface (Kudirka-144 well, 806 m depth); c) dolomite cement partially filling a vug within slightly fractured reef interval (Lapgiriai-1 well, 1130 m depth); d) silica-, siderite- and calcite-cemented fracture surface (Bliūdžiai-156 well, 949.8 m depth); e) large calcite crystals (up to 3 cm in length) growing within a dissolution enlarged fracture (Vilkaviškis-137 well, 804 m depth). Note the brown oil stains showing that fracture acted as a conduit to oil flow. (For interpretation of the references to colour in this figure legend, the reader is referred to the Web version of this article.)

CO_2-water-rock interactions are then run via thermo-chemical simulations for the rifogenic bodies within the Silurian reef belt in the Middle Lithuania (Fig. 1), that could serve as geothermal reservoirs for energy extraction. Natural deformation of Silurian carbonates is compared to simulation results to determine the most likely processes affecting the reservoir pore system at certain reservoir conditions.

1.1. Silurian reef structures in Lithuania and their geothermal potential

The Silurian carbonate reefal build-ups and patch reefs of Pridoli Minija regional stage were widely explored in the Middle Lithuania by the oil industry due to their potential for hydrocarbon accumulations. However, the discovered oil intervals are irregular, thin and local, and the detected reefogenic bodies are either “dry" or saturated with water and/or viscous oil (Zdanavičiūtė and Jacyna, 2003). Therefore, the oil has never been produced from the Silurian reefal structures because the oil production would not be economically viable. However, there are over 70 exploratory wells drilled through Silurian carbonate formations that are currently indicated as abandoned, plugged, buried and/or inactive, and thus could be re-used for geothermal purposes. Temperature for the top depth of the Silurian succession ranges from 25 to 38 °C with an average of around 32 °C for the reef structures. A recent study by Kaminskaite-Baranauskiene et al. (2024) evaluated geothermal potential of the Silurian reef structures and found that the heat production rates of well doublets within the reefs range from 0.000044 to 0.24 MWh, with two reservoirs worth considering for small geothermal projects: Kudirka and Pavasaris reefs (Fig. 1). They are the only reefs that have sufficient flow rates and high enough water availability within the closed structures. 6 well doublets arranged from the existing wells within the Kudirka structure could produce 2836 MWh during the heating season, whereas heating to the required district heating temperatures of >60 °C would increase the capacity of the doublets to around 1,580,000 MWh, which would cover the heating needs of the nearby towns and more. A doublet within the Pavasaris structure would produce 1056 MWh during the heating season, and the towns nearby with >1000 population would require around the same amount of thermal energy. Therefore, in this study CO_2-water-rock interaction modelling was done on those two most prospective reef structures.

2. Methodology

The results of this study came from integration of core logging and descriptions, macro- and microscopic petrography, cathodoluminescence and SEM microscopy, XRD testing and stable isotope analysis. Data on the formation water composition, as well as petrophysical properties of rocks were taken out from the oil industry reports held at the Lithuanian Geological Survey. Cored intervals from 53 wells that penetrated the Silurian carbonate succession of Middle Lithuania were described and logged. 150 hand specimens were selected for petrographic characterization, 95 of which were prepared for microstructural analysis. These data allowed identify the main deformation mechanisms and the relative timing of hydrothermal alteration. Rock and formation water characteristics data was then used for 2D and 3D water and CO_2-water-rock interaction modelling.

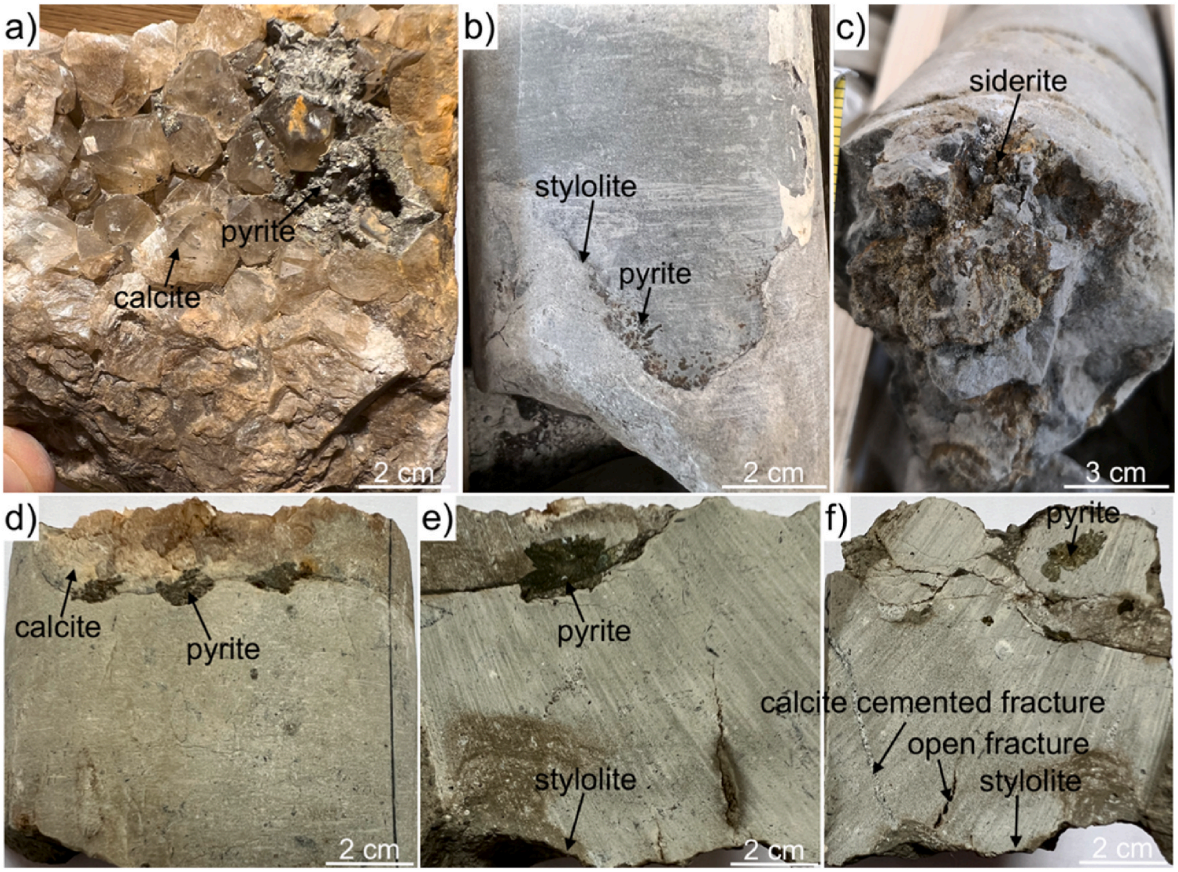

Fig. 6. Core photos showing precipitation of iron-rich mineral phases within the Silurian carbonates in Lithuania: a) pyrite precipitation alongside the calcite cementation on the surface of a fracture (Bliūdžiai-156 well, 935.6 m depth); b) pyrite dendrite structures forming on the stylolite surface (Bebirva-110 well, 969 m depth); c) siderite precipitating in the fractured interval of the reef also containing small silica crystals (Kurtuvėnai-166 well, 728.7 m depth); d-f) pyrite growing on the surface of a stylolite and replacing parts of the host rock and the calcite cement (Viduklė-61 well, 1169 m depth). Note the fractures growing perpendicular to the stylolite surface: one fully cemented and the other one fully open (f).

2.1. *Porosity, permeability and formation water analysis*

Lithostratigraphic data, borehole geophysical logs, drill-stem tests and core analyses were analysed for 53 hydrocarbon exploratory wells penetrating the Silurian carbonate formations of Middle Lithuania. Data on the chemical composition of Silurian formation water were collected from industrial reports of 3 wells: Vilkaviškis-135 well, representing Kudirka reef, Bliūdžiai-156 and Bedugnis-1 wells representing the reefs from the central Silurian reef belt in the Raseiniai area (Fig. 1; Cicha-Szot and Budak, 2016a, 2016b; Matyasik and Lesniak, 2016). The data includes water pH, electrical conductivity, dissolved solids at 180 °C, specific gravity and geochemical water content. Temperature data was taken from 15 wells measured at the top of the Silurian formation. Porosity and permeability data was assessed by interpreting the drill-stem tests from the wells together with the values measured on core samples. All the data comes from the well end reports held at the Lithuanian Geological Survey.

2.2. *Core and microstructural analysis*

The core intervals were analysed from 53 wells that penetrate the Silurian carbonate deposits. The macroscopic petrographic descriptions stem from observations of 150 hand specimens. A total of 95 thin sections were prepared for microstructural analysis from core samples containing hydrothermal products. They were examined under the plane-polarized and cross-polarized light using a Nikon Eclipse LV100N polarizing microscope (magnification 40 ×) and cathodolumine-scope model CITL Mk5-2 (~15 kV voltage and 350–400 mA current) at the Faculty of Chemistry and Geosciences, Vilnius university, Lithuania. Scanning electron microscopy analysis was performed at the Nature Research Centre, Lithuania, using the Quanta 250 instrument. Micrographs were taken using a backscattered electron detector. The chemical composition of minerals was obtained by the EDS detector X-Max, the INCA x-stream digital pulse processor and the INCA Energy EDS software.

2.3. *X-ray diffraction analysis*

X-ray diffraction (XRD) analyses were performed on 63 samples collected from the wells representing different types of host lithofacies within the hydrothermally altered carbonate intervals. Three grams of collected samples were smashed into powders of 300 meshes and compressed into a solid specimen. Then, the solid specimen was fixed into the sample box of the D8 DISCOVER X-ray diffractometer in the National Research Centre for Geoanalysis (NRCGA) at Chinese Academy of Geological Sciences. Detail measuring and analysing procedures were in accordance with Li et al. (2019, 2021). Mineralogical characteristics of different lithofacies were used in the thermo-chemical modelling.

2.4. *C and O stable isotope analysis*

25 samples were analysed using C and O stable isotope tests to evaluate the temperature conditions at which different structures have formed. Small plugs were collected from the cements and vug/vein-fillings of interest by using a dentist's drill, and then smashed into powders of 200 meshes. In order to release CO_2, about 50 mg powders

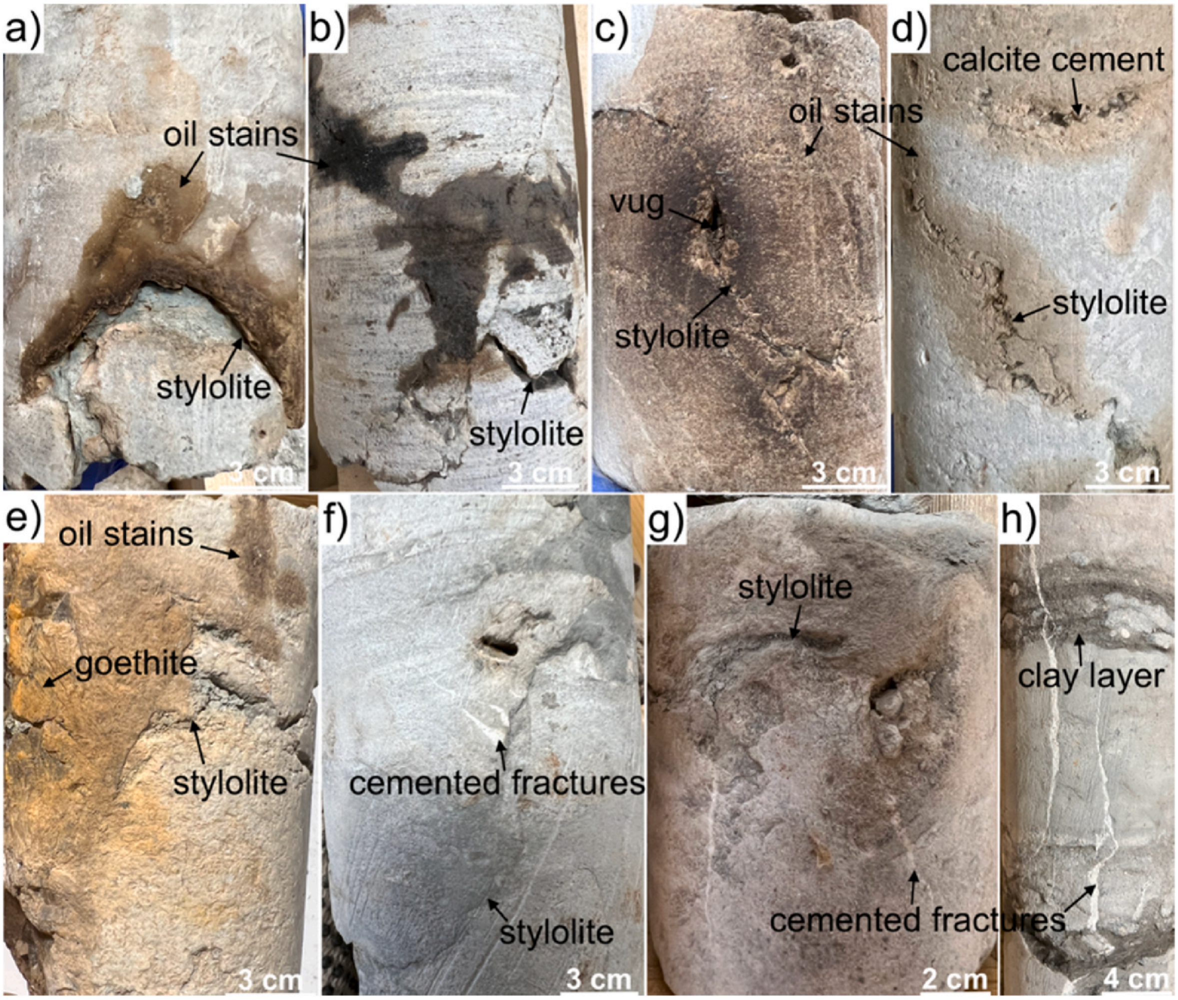

Fig. 7. Core photos showing stylolite and clay seam related structures formed within the Silurian carbonates in Lithuania: a) stylolite surface that acted as a conduit to oil flow parallel to the stylolite surface (note brown oil stains above the stylolite surface) and a barrier to oil flow perpendicular to the stylolite due to clay accumulations (Kudirka-1 well, 766.2 m depth); b) open fractures formed due to irregular indentations of a stylolite all of which acted as a conduit to oil flow (Vilkaviškis-136 well, 807.9 m depth); c-d) stylolite surfaces that were enlarged by dissolution resulting in the formation of vugs along the stylolite surface. Note oil stains saturating the rock away from the stylolite surface (c) Kudirka-1 well, 809 m depth; d) Vilkupiai-1 well, 787 m depth); e) stylolite acting as conduit to oil flow (i.e. oil stains) and fluid flow rich in iron phases (i.e. precipitation of goethite) (Bliūdžiai-156 well, 935.6 m depth); f-g) fracture/veins formed due to the escaping dissolved calcite at the stylolite surface (Tidikas-1 well, 1055–1065 m depth). The veins are fully cemented by calcite; h) fractures/veins formed perpendicular to clay seams and are fully cemented by calcite (Lapgiriai-1 well, 1035 m depth). (For interpretation of the references to colour in this figure legend, the reader is referred to the Web version of this article.)

were put into a vacuum to react with 100% phosphoric acid at 25 °C for 24 h. The CO_2 was collected and measured for stable carbon and oxygen isotopes on a Finnigan MAT251 mass spectrometer at the Stable Isotope Laboratory, Institute of Geology and Geophysics, Chinese Academy of Sciences. Data for stable carbon and oxygen are reported in per mil relative to the Vienna Peedee Belemnite (VPDB) standard. The precision for $\delta^{13}C$ and $\delta^{18}O$ measurement is ±0.1‰.

2.5. *Inclusion analysis*

Fourteen thin sections were prepared to study fluid inclusions in calcite cement in Silurian carbonate formation. Six samples were derived from veins, two from inter- and intra-particle cement, and six from sparry cement within vugs. The type, size, and shape of fluid inclusions in calcite were evaluated under the Leica DM4P polarizing microscope. The microthermometry of liquid-vapour two-phase inclusions in calcite was measured using the Leica DM4P polarizing microscope and the LINKAM THMS600 heating/freezing stage at the Beijing Research Institute of Uranium Geology, China. The temperature range of the cooling and heating stages was controlled from −100 °C to 200 °C, with an accuracy of 0.1 °C. In the initial heating stage, the heating rate was 10 °C/min. The changes in fluid inclusions during heating were observed. At temperatures close to the measured phase-change temperature, the heating rate was reduced to 1–2 °C/min, and the temperature at which the vapour phase disappeared in the fluid inclusion was recorded. During the freezing process, the heating/freezing stage was cooled to the predetermined temperature and then warmed naturally, recording the melting temperature of the fluid inclusion. During the process of measuring the homogenization temperature and melting temperature, a "cycle" test was used to improve accuracy. The cycle included around 2–3 repetitions, and the average homogenization temperature and average melting temperature were recorded. Using the NaCl-H_2O system data from Bodnar (1993), the salinity of the liquid phase in the inclusion was calculated according to the measured melting temperature.

2.6. *Water-rock interaction modelling*

CO_2-water-rock interactions were evaluated in two steps. First, the saturation states of minerals in Silurian formation water were computed

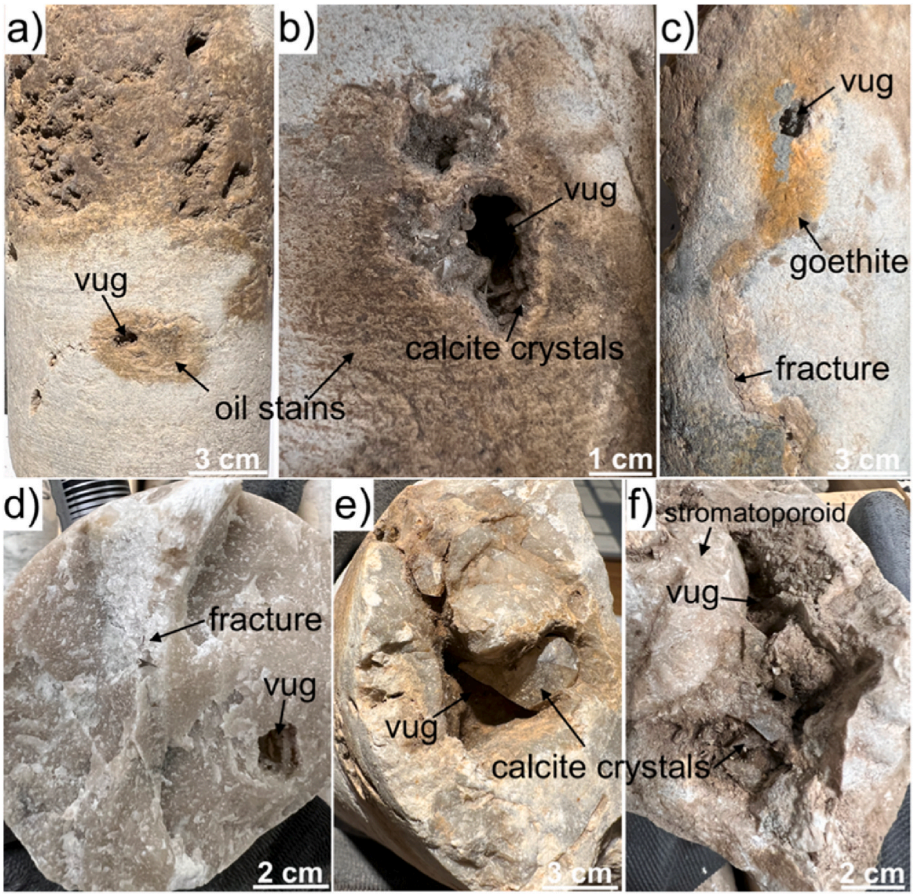

Fig. 8. Core photos showing dissolution products within Silurian reef structures in Lithuania: a) vuggy interval saturated with oil (brown stains), the vugs are fully open (Vilkaviškis-137 well, 811.2 m depth); b) vugs encrusted with calcite cement (Vilkaviškis-136 well, 780 m depth); c) vug formed along a fracture surface due to dissolution, the fracture is partially stained with goethite (Bliūdžiai-156 well, 947.4 m depth); d) fracture and vug within the microcrystalline dolostone encrusted with tiny calcite crystals (Vilkaviškis-137 well, 824.6 m depth) e) vugs containing large (up to 5 cm in length) calcite crystals (Vilkaviškis-136 well, 832.6 m depth); f) dissolution enlarged pores around the stromatoporoid walls, the vug surface is partially encrusted with calcite cement (Kudirka-147 well, 818 m depth). (For interpretation of the references to colour in this figure legend, the reader is referred to the Web version of this article.)

at reservoir and injection temperatures using the PHREEQC code with the phreeqc.dat as the selected database. This allowed us to determine which mineral phases are in equilibrium with water and which ones would likely be dissolving or precipitating. Next, a formation water composition was numerically reacted with the host rock mineralogy at reservoir and injection temperatures using TOUGHREACT.

TOUGHREACT is a software program widely used to simulate the fluid-flow and chemical reactions of fluids in underground environments. Unlike simpler models, it can account for complex conditions like fractures, variable temperatures, and the chemistry of the fluids themselves. Originally written in FORTRAN77, it integrates with TOUGH2 to handle a wide range of factors including pressure, temperature, pH, and salinity (Xu et al., 2006). TOUGHREACT solves fluid flow equations for each section of the simulated environment, considering principles of mass balance, momentum balance, and energy balance.

Using this methodology, the evolution of fluid and rock compositions with time could be evaluated and compared with the observed present-day water and rock compositions of the Silurian hydrothermal system.

The data used for the geochemical modelling include major ion chemical composition and pH, Eh, density and temperature of the formation water. The following major mineral phases were considered:

- Sulphates (gypsum, anhydrite)
- Carbonates (calcite, aragonite, dolomite)
- SiO_2 phases (amorphous, chalcedony)
- Iron hydroxides (goethite, amorphous $Fe(OH)_3$).

The program calculates saturation indices (SI) from the following equation:

$$SI = \log(IAP / K) \tag{1}$$

where IAP is ion activity product, K – equilibrium constant,

$$IAP = [A][B] \tag{2}$$

$$K = [A'][B'] \tag{3}$$

where A, B are activities of species A, B in the water sample, A′, B′ activities at equilibrium.

The saturation indices, *SI*, were calculated for individual mineral phases and temperatures. The negative values show formation water undersaturation with respect to the given mineral, expected to dissolve it in the solution, whereas positive values show water supersaturation therefore a given mineral is expected to precipitate. In case SI = 0, the fluid and the mineral phase are in chemical equilibrium.

Using TOUGHREACT, 3D models were constructed with doublet wells (a production and an injection well) in the following reef intervals (three different cases were simulated for comparison):

- Calcite-rich Kudirka reef interval (Kudirka-144 and Vilkaviškis-137);
- Dolomitized Kudirka reef interval (Vilkaviškis-135 and Vilkaviškis-126);

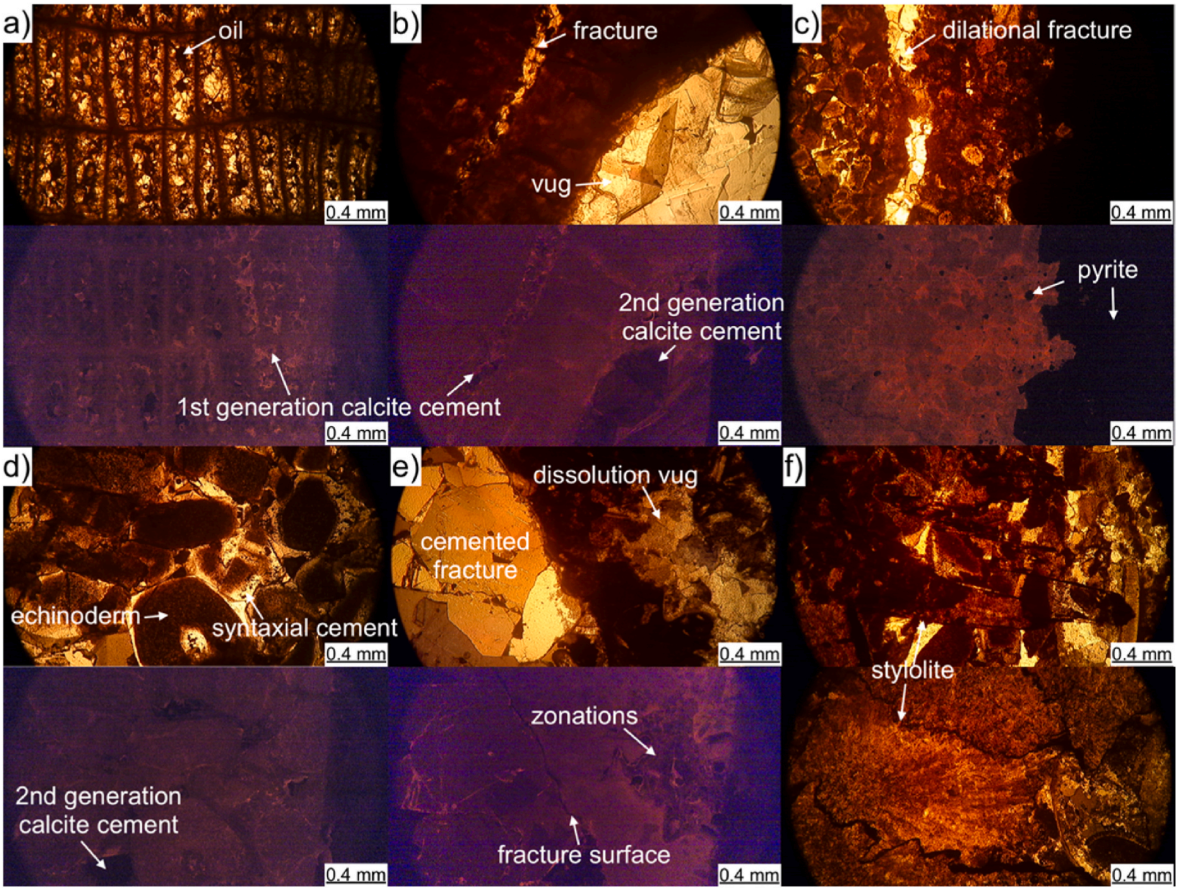

Fig. 9. Microphotographs under plane-polarized and CL light (CL images are under the optical micrographs except (f) where both are optical images): a) intragranular pores within the bryozoan the surfaces of which are encrusted by calcite cement and the remaining pore space is filled with oil (black); b) fracture/vein and vug filled with calcite cement; the black spots within the fracture are oil stains; the cements within the vugs show two generations: 1st generation, forming a fringe of isopachous, scalenohedral crystals; and 2nd generation comprising rhombohedral crystals; c) pyrite-rich packstone/grainstone with a cemented dilational fracture; pyrite has formed either as single crystals or aggregates made up of tiny framboid crystals (black under optical and CL light); d) typical echinoderm-rich grainstone that is intensely cemented by syntaxial cement around the echinoderms; e) fracture enlarged vug filled with large rhombohedral calcite crystals, and dissolution vug showing several cementation stages under the CL light: brighter and darker orange luminescence zones growing from the wall rock into the centre of the vug; f) stylolites showing dissolution of fossils and a layer of micrite and clay (insoluble material - black). (For interpretation of the references to colour in this figure legend, the reader is referred to the Web version of this article.)

- Calcite-rich Pavasaris reef interval in the Raseiniai reef zone (Bliūdžiai-156).

The simulations employed a constant production and injection rate of 5 kg/s. Table 1 summarizes the physical properties of the rock formations used in the modelling. The mineral compositions are given in Table 2. Within TOUGHREACT, reaction rates and activation energies of the minerals are crucial parameters for quantifying water-rock interactions and are shown in Table 3.

Aqueous speciation calculations were performed using PHREEQC to identify the relevant aqueous complexes governing CO_2-water-rock interactions within the TOUGHREACT simulations (Table 4).

3. Results

3.1. *Silurian carbonate formation characteristics*

Studied Silurian carbonate formation is mainly composed of massive microcrystalline limestone and clayey microporous limestone, often intensely stylolitized, whereas effective reservoir rocks of reefal buildups mostly consists of stromatoporoid, crinoid and detrital limestone with admixture of fauna such as brachiopods and corals. Some of the formation intervals are also dolomitized, dolomitized rock sections reaching several meters in thickness. The thickness of the reefal buildups may reach up to *c.*90 m, however, the effective thickness of the reservoirs ranges within several meters and rarely reaches 20 m (Kaminskaite-Baranauskiene et al., 2024). That is because of the high heterogeneity of the structure and hence the poor connectivity between different types of porosity such as vugs and intraporosity system. The most prolific reef sections are fracture-dominated, heavily stylolitized intervals or layers affected by enhanced dissolution forming vuggy porosity. That can be proved by oil stains observed on the cores taken out from the wells. Some of the effective layers are also dominated by matrix porosity associated with the lithologies characterised by best petrophysical properties such as crinoid-stromatoporoid-detrital limestones. However, open porosity of these limestones is still mostly <10 %, and permeability <10 mD.

4. Host rock mineralogy

XRD results show that host rocks in most of the reef reservoirs are largely made up of calcite and iron-rich dolostone (>70 %) (Fig. 2). Most of the samples also contain smaller amounts of quartz (0.1–27.78 %) and clays (0.4–35 %). Anhydrite and gypsum are observed in half of the samples in amounts varying from 0.25 to 32 %. At least third of the samples contain 0.1–13.5 % pyrite and siderite. Minor amounts (<5 %)

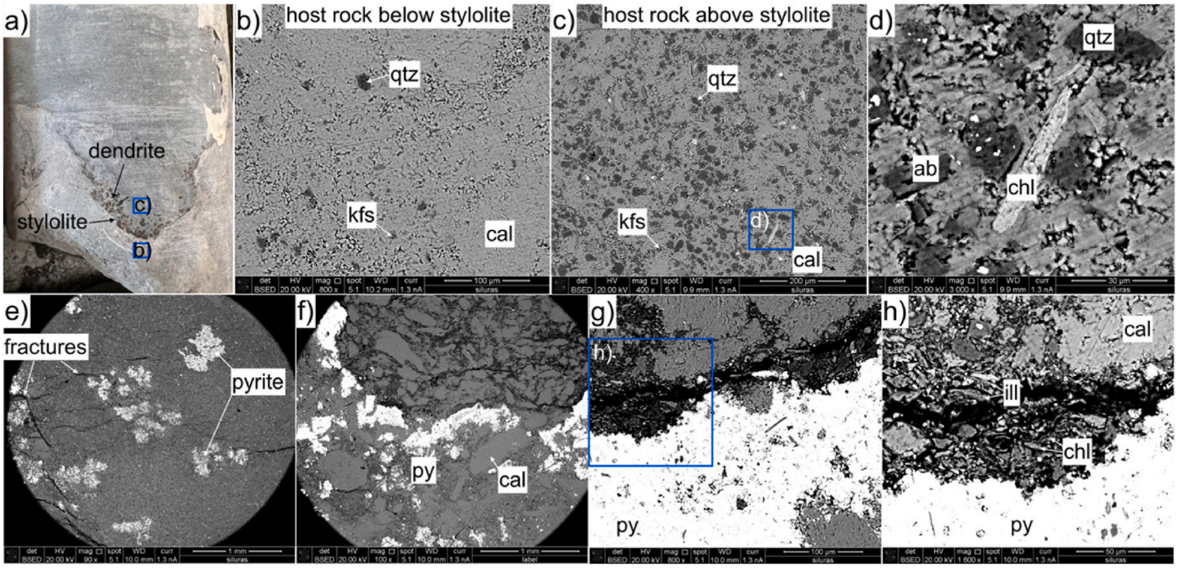

Fig. 10. Example of a stylolite surface showing dendrite structures of pyrite. a) Core photograph of the stylolite, where sample for BSEM analysis was taken from; b) BSEM image of the host rock below, and c) above the stylolite surface to show that host rock above stylolite contact has a much higher density of quartz particles compared to the rock below the stylolite; d) is a zoomed in image showing chlorite (chl), albite (ab) and quartz (qtz) minerals within the host rock above the stylolite; e) BSEM image showing fractured zone around stylolite and pyrite precipitations at the ends of those fractures; f) stylolite surface, showing a sharp boundary between pyrite precipitations on one side of the stylolite surface and no precipitations on the other side; g-h) zoomed in images of the stylolite surface showing precipitations of clay minerals (illite (ill), chlorite (chl)). Blue rectangles show position of the zoomed in BSEM images. (For interpretation of the references to colour in this figure legend, the reader is referred to the Web version of this article.)

Table 5
Geochemical data of the formation water from several wells penetrating Silurian reef structures used for modelling.

Well	pH	Dissolved solids at 180 °C	Cl	Br	J	HCO_3	SiO_3	SO_4	Fe_{tot}	Ca	Mg	NH_4	Na	K
Bedugnis-1	6.4	99.3	60.128	0.533	0.003	0.327	0.095	1.292	0.189	8.247	2.858	0.01	27.8	1.01
Vilkaviškis-135	6.7	74.1	45.309	0.191	0.003	0.375	0.029	0.652	0.364	4.673	2.019	0.048	20.07	0.525
Bliūdžiai-156	6.5	106.2	60.607	0.33		0.085		0.603		9.05	2.648		24.49	0.427
K. Naumiestis-43		76.2	46.458	0.194	0.0004	0.121		0.121	0.005	3.65	2.384		21.75	0.371
Vilkaviškis-137		75.8	44.409	0.19		0.161		0.61		3.879	2.321		20.48	0.268
Vilkaviškis-126		75.5	45.075	0.181		0.186		0.125		3.706	2.027		21.448	0.266

of plagioclase, K-feldspar, analcite and halite are also found.

5. Stable isotope results

Samples exhibit large magnitude variation in $\delta^{13}C$ and $\delta^{18}O$, ranging from −5.3‰ to 1.8‰ for $\delta^{13}C$ with an average of −0.5‰, and −16.2‰ to −1.9‰ for $\delta^{18}O$, with an average of −5.7‰ (Fig. 3). $\delta^{13}C$ and $\delta^{18}O$ of dolomite crystals show correlation, with $\delta^{13}C$ ranging from −2.4‰ to −0.6‰ and $\delta^{18}O$ ranging from −5.2‰ to −2.2‰. $\delta^{13}C$ and $\delta^{18}O$ values of calcite within the vugs are also within a cluster, with $\delta^{13}C$ ranging from −0.7‰ to 1.8‰ and $\delta^{18}O$ ranging from −4.7‰ to −2‰. $\delta^{13}C$ and $\delta^{18}O$ of calcite within veins show no clear correlation, with $\delta^{13}C$ ranging from −5.3‰ to 1‰ and $\delta^{18}O$ ranging from −16.2‰ to −2.4‰. Gypsum precipitates show similar $\delta^{13}C$ values (−0.3–0.9‰) and widely scattered $\delta^{18}O$ values (−16.2 to −2.3‰). Overall, $\delta^{18}O$ values are all negative and do not reach higher values than −1.9‰. $\delta^{13}C$ values increase from calcite within veins, to dolomite crystals indicating dolomitization process, then gypsum precipitates and calcite within vugs.

5.1. Inclusion results

The inclusions used in microthermometry are all vapour-liquid two-phase fluid inclusions. The measured inclusions are all those within the calcite cement, which are fluid inclusions trapped simultaneously during the precipitation of the calcite cement. They often occur in groups parallel to certain crystallographic directions of the host mineral. Therefore, they are primary inclusions. They are liquid-rich fluid inclusions, because the vapour/liquid ratios range from 5% to 20%. The vapour/liquid ratios of the inclusions in the inter- and intra-particle calcite cement are less than 5%, with inclusion sizes of 5–30 μm, and the salinity varying from 0.35 wt% to 23.18 wt%. The vapour/liquid ratios of the inclusions in the sparry calcite cement within vugs range from 5% to 10%, with inclusion sizes of 5–35 μm, and the salinity varying from 0.71 wt% to 23.18 wt%. The vapour/liquid ratios of the inclusions in the veins range from 5% to 20%, with inclusion sizes of 5–35 μm, and the salinity varying from 0.35 wt% to 21.47 wt%. The homogenization temperature of the inclusions in the Silurian carbonate formation was distributed within the range of 70–140 °C (Fig. 4). The highest precipitation temperature peak zone of intra-, inter-particle calcite cement is around 70–75 °C. The precipitation temperatures of calcite cement within vugs is divided into two peak zones, one is about 90–100 °C and the other is about 120–140 °C. The precipitation temperatures of veins show only one peak, that is approximately 120–130 °C.

6. Hydrothermal alterations

6.1. Mineral substitution and precipitation

6.1.1. Carbonate cementation

Fractured intervals within the studied carbonates always show at least partial calcite cementation. Calcite cement is found in various

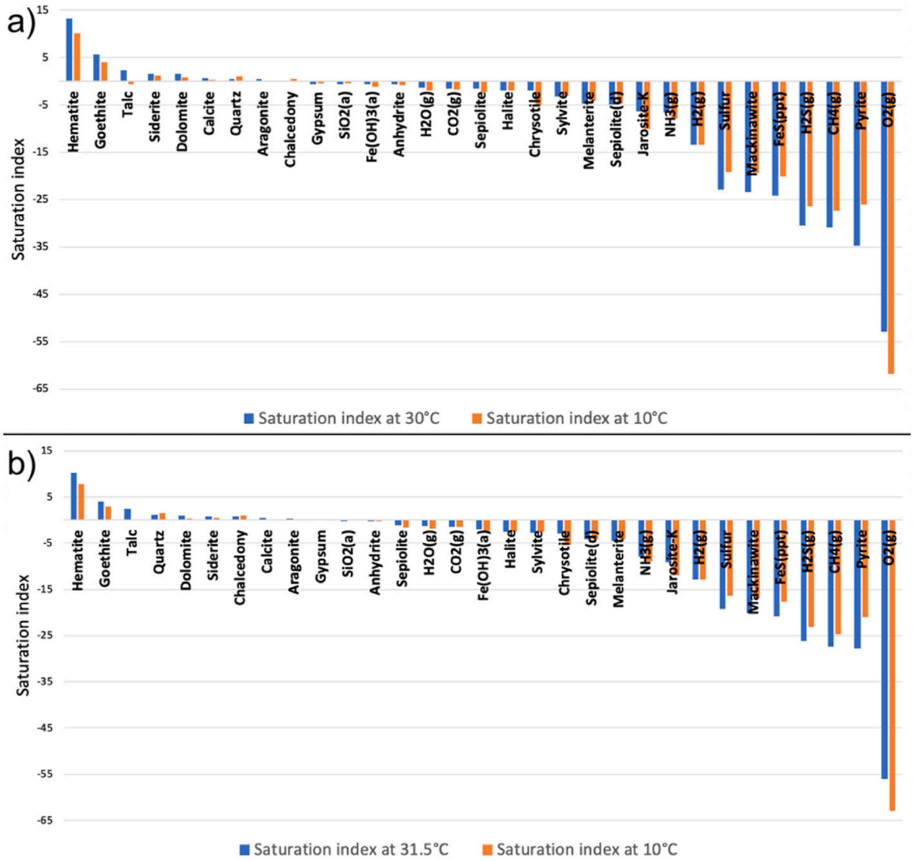

Fig. 11. Figure illustrating saturation indices of various mineral phases within formation water in 2 different wells penetrating the Silurian carbonate reefs: a) Vilkaviškis-135 well, and b) Bedugnis-1 well.

forms: in veins (Fig. 5a), as large individual calcite crystals growing in dissolution enlarged fractures (Fig. 5e) and vugs (Fig. 8e), and as calcite cement encrusting fracture (Fig. 5b–d; Fig. 6a; Fig. 8d) or vug surface (Fig. 8b–d). Dolomite cement is rare but also observed in a few vugs and fractures (Fig. 5c). Siderite, pyrite and silica crystals are also observed precipitating alongside the calcite cement (Fig. 5d; Fig. 6a–f).

6.1.2. Dolomitization

The average amount of dolomite in the analysed wells is *c.*7 %, varying between 3 % in the Raseiniai reefs at a depth of >900 m and up to 20 % in the Kudirka reef at a depth of >770 m. The level of dolomitization varies greatly between the wells even within a single reef. For instance, the amount of dolomite in Vilkaviskis-131 and Vilkaviskis-135 wells is significantly increased compared to the other wells in the Kudirka reef. As shown by core analysis, dolomitization is generally associated with secondary fractures and stylolitization surfaces. Therefore, structurally deformed intervals indicate higher levels of dolomitization.

6.1.3. Iron

The average iron mineral content of the rocks is *c.*1 %. It varies in amount throughout the wells, with maximum iron mineral content (>5 %) observed in Pavasaris reef (Bliudziai-156 and Tidikas-1 wells), as well as Vilkaviskis-131 well (>3 %) within the Kudirka reef. Iron is found in many forms, but mostly as pyrite and siderite, less often as goethite stains (Figs. 6, 7e and. 8c). Pyrite was observed in almost all the wells. In general, pyrite crystals are observed in the insoluble residue on stylolite surfaces (Fig. 10), sometimes forming wavy rows of pearls (Fig. 6d–f). Pyrite particles are also common in the micritic matrix, varying in size from a few μm to mm, either as single crystals or aggregates made up of several crystals (Fig. 9c). Pyrite crystals are also observed within the sparry calcite cement within the vugs and fracture surfaces (Fig. 6a). There pyrite can form aggregates of up to 5 cm in width. Siderite is also commonly observed within the fractured core intervals, precipitating on fracture surfaces together with calcite and silica cement (Fig. 5d; Fig. 6c).

6.1.4. Silica

Calcite-replacing silica crystals were observed in some samples within the micritic matrix (Fig. 10). They are a few μm in size and scattered as single crystals. The presence of residues of micrite within many of the crystals shows that they are of an authigenic nature.

6.2. Stylolitization

Some of the intensely stylolitized reef intervals (e.g., Bliūdžiai-152 well) are heavily dolomitized suggesting that stylolites acted as conduits to dolomitizing fluid flow. Moreover, stylolite surfaces acted as precursors for fracturing both due to the formation of irregular stylolite indentations (Fig. 7b) and due to escaping fluids from the dissolution of calcite along the stylolite surface (Fig. 7f and g). Fractures formed perpendicular to stylolites or seams are short and often mineralised with calcite, although some open fractures were also observed (Fig. 7f–h). Moreover, some stylolite related fractures spread forming up to 1 m thick fracture zones around the stylolite surfaces (Fig. 7b). Diagenetic minerals and oil stains along stylolites and seams suggest that stylolitization and related fracturing acted as conduits to fluid flow (Fig. 7).

6.3. Dissolution

Dissolution forming cavernous/vuggy porosity is common in majority of the studied wells. Together with stylolitized and fractured

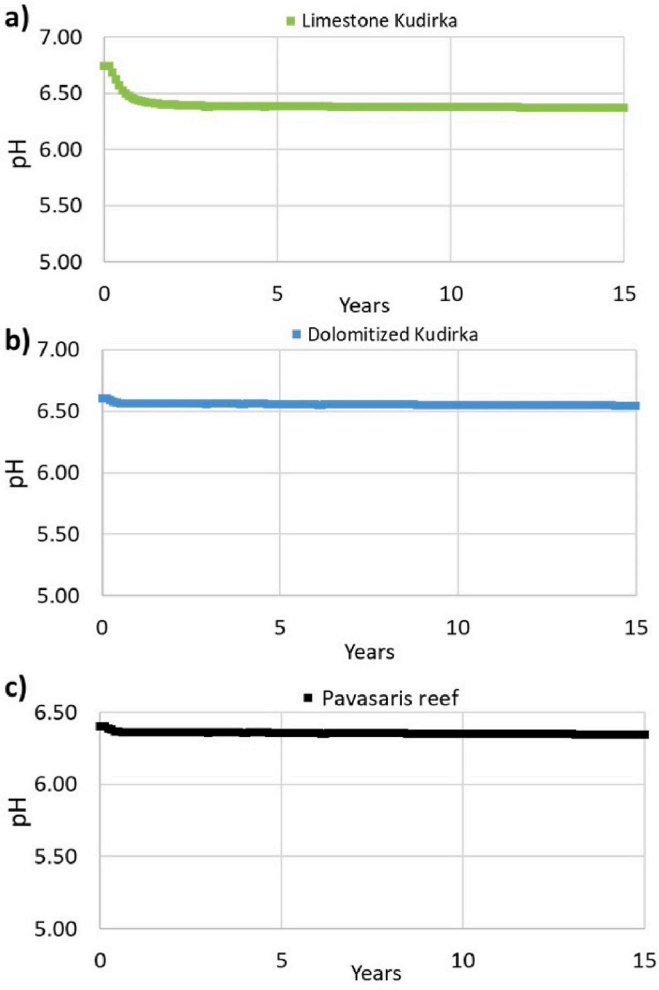

Fig. 12. pH changes in the reinjection well for a 15-year interval for the studied: a) calcite-rich Kudirka; b) dolomitized Kudirka, and c) Pavasaris reef intervals.

intervals it forms the most proliferous zones within the reefs (Fig. 8a and b). Dissolution is fracture related, but also common in stromatoporoid limestone. Stromatoporoid limestone has high intraporous porosity that led fluid flow and hence dissolution around the stromatoporoid fossil walls, further increasing the rock's permeability (Fig. 8f). Vugs are also observed within detrital and crinoid matrix-supported limestones, as well as microcrystalline dolostones, where microporous fabric relates to a loss of volume associated with dolomitization forming intercrystal porosity as a precursor for dissolution (Fig. 8d).

6.4. Microstructural analysis: rock deformation

Porosity and permeability within the Silurian reefs in the Middle Lithuania have been degraded by the precipitation of inter- and intragranular cement but were enhanced by late diagenetic leaching. Crinoidal and detrital grainstones are mostly made up of echinoderm fragments that acted as substrates for the syntaxial calcite cement greatly reducing the primary intergranular pore space (Fig. 9d). The vugs and fracture surfaces are cemented by two generations of spar: an earlier with an isopachous, scalenohedral crystals, and a later one with rhombohedral crystals (Fig. 9b). Dissolution vugs are very common throughout the studied carbonates, as well as solution-enlarged pores and tension gashes (Fig. 9e). Fractures which temporally increased porosity were filled with calcite and rarely dolomite cement (Fig. 9b–e). The remaining pore space of the solution vugs, caverns and fractures is largely saturated with oil (Fig. 9a and b). The non-carbonate minerals observed under the microscope were pyrite in the form of microcrystalline framboid crystals or their aggregates (Fig. 9c) and trace authigenic quartz crystals (Fig. 10b–d). They are replacing the pre-existing calcite along stylolite surfaces, fractures and around vugs. Pyrite and silica are also observed within the rock's matrix, however their particle size is always very small (<0.1 mm) compared to the ones growing along stylolites and fractures, where they may reach up to 0.5 cm in diameter (Fig. 10). Clay particles forming pockets and lamina concentrations were observed along the stylolite surfaces (Figs. 9f and. 10 g–h) or scattered within the rock's matrix.

6.5. Silurian formation water chemistry

Dissolved solids from the formation water at 180 °C varies between 74.1 g/l at the largest Kudirka reservoir (Vilkaviškis-135 well) to 106.2 g/l at the small Pavasaris reef structure in the Raseiniai area (Bliūdžiai-156) (Table 5). The water is slightly acidic in all reservoirs (pH of 6.4–6.7). The Silurian water is rich in chlorides (45–61 g/l), calcium (3.7–9 g/l) and magnesium (2–2.9 g/l). Sulfates are at low concentrations, varying between 0.19 and 2.68 g/l. The degree of metamorphism is 0.49–0.78 (Na/Cl, mg/l). Electrical conductivity ranges between 97.6 and 152 mS/cm, and specific gravity is 1.053–1.098 g/cm^3. The Silurian formation water is thus 7.4–13.6 % brine, hydrogeochemical indicators indicate that the water is ancient residual sea water and has been accummulated in well hydraulically isolated layers. The sampled water is slightly yellow in colour, opalescent and has a film of brown oil on the surface.

6.6. Phreeqc results

Negative values of the saturation index, *SI*, indicate formation water undersaturation, where minerals are expected to dissolve, whereas positive values show water supersaturation, where minerals are expected to precipitate from that solution. PHREEQC simulation results show that at current reservoir temperature, formation water in most of the reef structures is supersaturated with oxides (hematite), hydroxides (goethite) and silicates (talc, quartz, chalcedony) (Fig. 11). SI values of carbonate minerals (calcite, dolomite, siderite, aragonite) varies throughout the wells but it is always close to zero. The formation water is slightly undersatured or in equilibrium with ahydrite, halite and gypsum in all studied wells. The largest undersaturation in all the wells is typical for Fe-sulphides (pyrite FeS2, mackinawite FeS, FeSppt). Most important result of geochemical simulation is presence of great variety of iron species in formation. SI of hematite and goethite is always positive, whereas SI of Fe-sulphides is always very low and negative, siderite shows either slightly positive or negative SI values. SI for salt is around zero indicating chemical equilibrium.

Results show that when water cools down to 10 °C at injection, the saturation indices slightly change. Most commonly supersaturation of hematite, goethite and siderite decreases, undersaturation of Fe-sulphides decreases, water saturation state in respect to silicates (quartz, chalcedony) slightly increases, whereas saturation of carbonate minerals decreases (Fig. 11).

6.7. Water-rock interaction modelling

To assess the impact of cold water injection on mineral alteration, a constant injection temperature of 10 °C was maintained for a 15-year simulation period, encompassing both the near-wellbore and deeper reservoir regions. Simulations of the pH changes in the reinjection well show a slight drop in the values in all simulated reef intervals after the first 0.5–1 year of injection and almost constant values after that (Fig. 12). The largest drop is observed in the calcite-rich Kudirka reef interval where the starting pH values were the highest (pH = 6.8), dropping to 6.4 after the 1 year of injection.

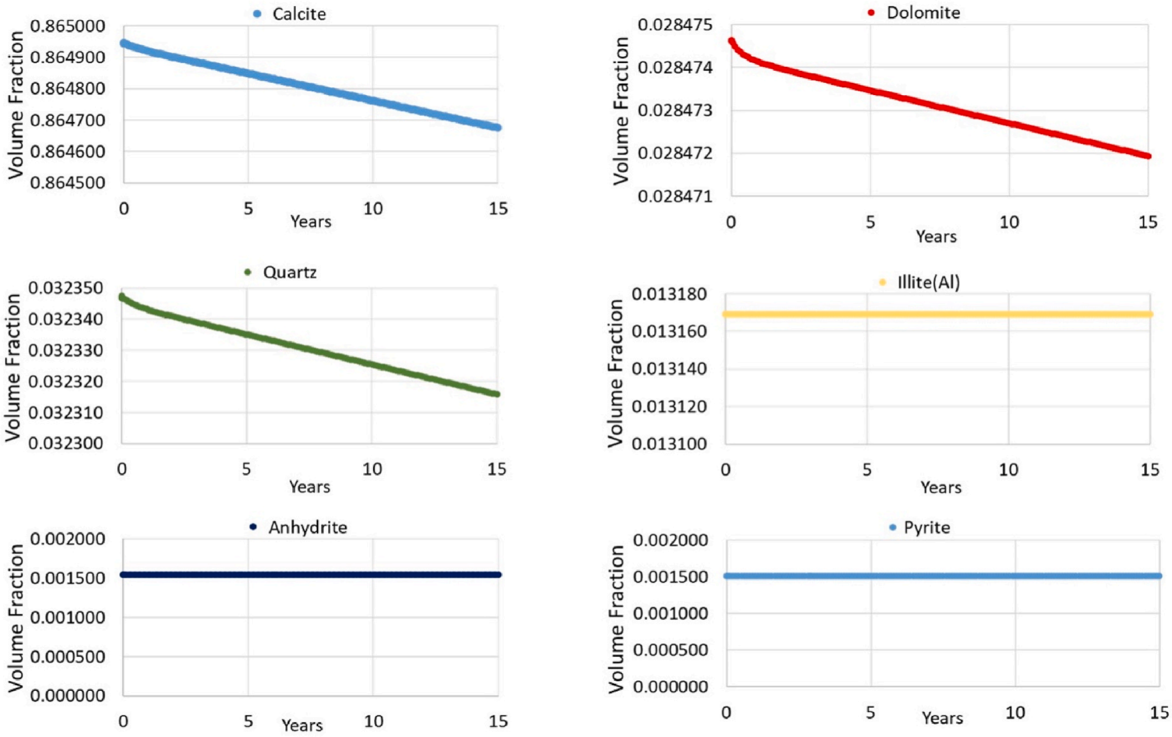

Fig. 13. Changes in the mineral volume fraction of the calcite-rich Kudirka reef interval after 15 years of CO_2-water-rock interaction simulations.

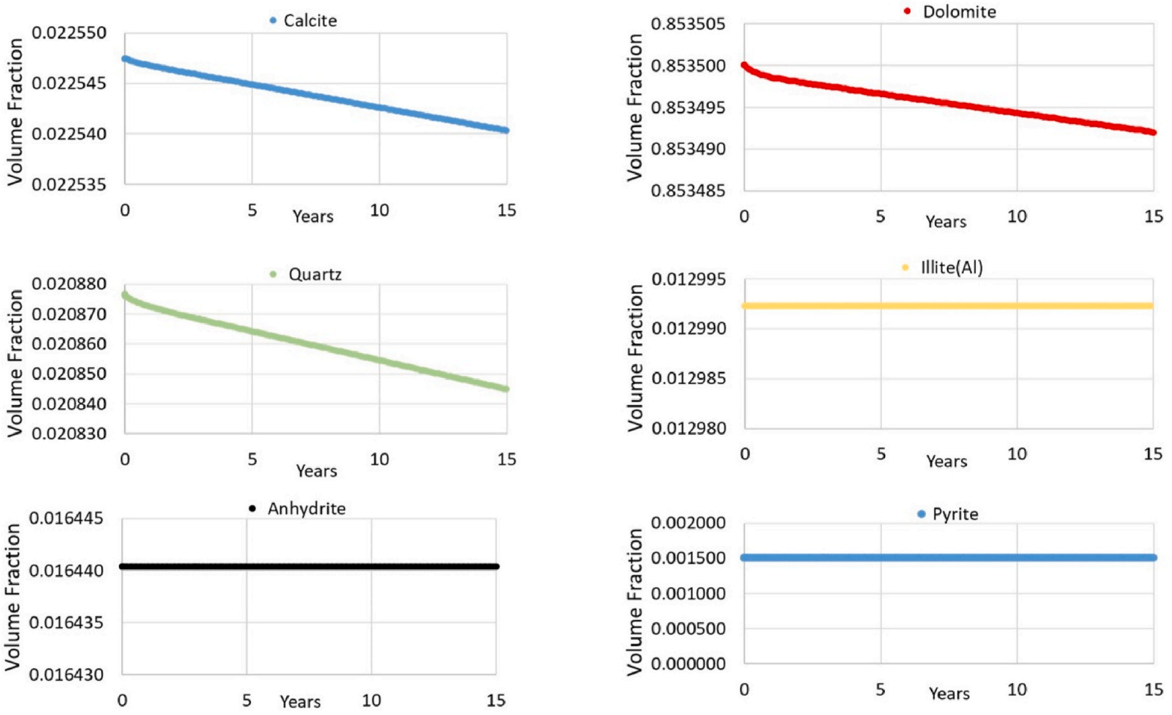

Fig. 14. Changes in the mineral volume fraction of the dolomitized Kudirka reef interval after 15 years of CO_2-water-rock interaction simulations.

3D simulation results show that the dissolution of dolomite and calcite are the dominant reactions during the whole process of CO_2-water-carbonate interactions for all cases (Figs. 13–15). In the calcite-rich reef intervals, Ca^{2+} increases slowly at the very beginning of the simulation and starts to decline after about 0.5 years. Similarly, Mg^{2+} also increases slowly in the early stage, but the increase accelerates after 0.1 years. In the dolomitized reef interval, dolomite shows lower volume fraction changes compared to calcite decrease in the calcite-rich intervals (Fig. 14). There is little volume change of anhydrite, pyrite and illite minerals in both the calcite-rich and dolomitized Kudirka reef intervals. Slight decreases with time are observed for anhydrite and illite minerals in the Pavasaris reef. Similar decreasing volumes of quartz are observed in all studied reef intervals.

Based on spatial variation of minerals within the calcite-rich

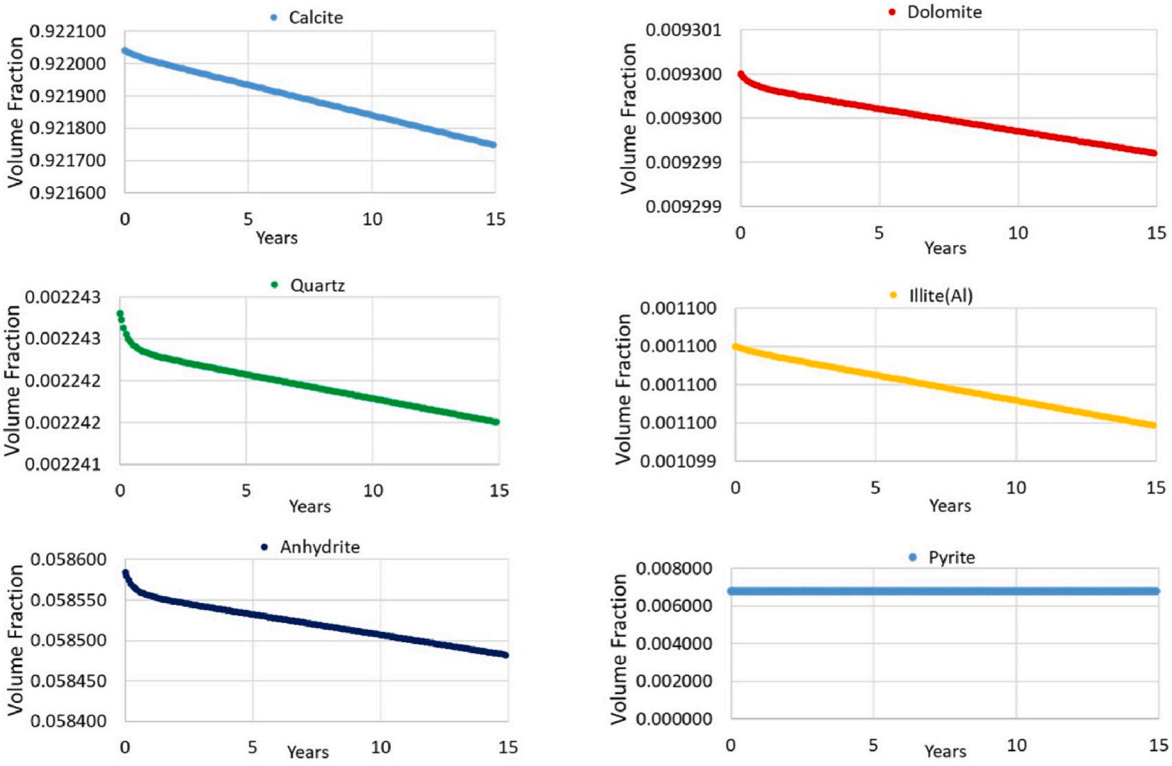

Fig. 15. Changes in the mineral volume fraction of Pavasaris reef interval after 15 years of CO_2-water-rock interaction simulations.

Pavasaris and Kudirka reef intervals after the 15 years of CO_2-water-rock interaction simulations, a slightly increased calcite and anhydrite dissolution is observed around the injection well compared to the surroundings of the production well, whereas changes in dolomite, illite and pyrite distribution are negligible (Fig. 16). In the dolomitized Kudirka reef, an increase in calcite and dolomite dissolution is observed around the injection well, as well as a minor increase in quartz dissolution, whereas negligible changes were observed for illite, anhydrite and pyrite minerals (Fig. 17).

7. Discussion

7.1. *Pore evolution and timing of hydrothermal events in Silurian carbonates*

The hydrothermal alteration of carbonate deposits involves complex physicochemical processes of interaction with warm/hot fluids, promoting various processes including dissolution as well as mineral substitution and precipitation. These processes indicate the existence of permeable pathways to allow the percolation and interaction of fluids (e.g., Davies and Smith Jr, 2006; Mansurbeg et al., 2016). Hydrothermal activity is very common within the Silurian carbonate formation. It mainly presents widespread dolomitization, intense dissolution forming vugs and caverns and solution-enlarged stylolites, associated tension-gashes as well as fractures, and various types of hydrothermal mineral deposits, such as calcite, dolomite cement, quartz, siderite and pyrite precipitations. The presence of diagenetic minerals and oil stains is found within the primary rock fabric (inter- and intra-granular pores), along stylolites, fractures as well as vugs and caverns of various sizes. That suggests that stylolitization and related fracturing formed pathways for fluid flow.

Very few previous studies dealt with the diagenetic alterations of the Silurian reefs and their impact on rock properties. Stentoft et al. (2003) studied the relative timing of diagenesis at the largest Kudirka reef in Lithuania, providing burial history of the area shown in Fig. 18, and our results are supported by their conclusions. The thermal history of the Baltic basin hasn't been studied in great detail, although a study by Lazauskiene and Marschall (2002) provides insights on thermal evolution of the Lower Palaeozoic sediments in Lithuania. The authors tested chitinozoan reflectivity in 12 wells in the E-W oriented profile across Lithuania providing a series of thermal maturity profiles. The observations showed thermal overprints on the normal thermal maturity gradients, suggesting episodes of high temperature fluid flushes during the development of the Baltic basin. Increased paleotemperatures effecting Late Silurian intervals showed values as high as 130–150 °C (Lazauskiene and Marschall, 2002).

Reconstruction of the relative timing of the hydrothermal processes within the Silurian carbonates suggests that soon after the primary lithification of the rock, primary rock fabric was cemented by syntaxial cement mainly overgrowing fragments of echinoderms (Fig. 18). Intra- and inter-porosity cementation took place soon after that, destroying large part of the primary porosity within the fossils and between the grains. Based on inclusion analysis of the intra- and inter-particle cement, thermal event must have taken the place during this time forming pretty high formation temperatures for such shallow depth (70–75 °C). This could be explained by the continental-continental collision and progressive burial since Late Silurian and during much of the Devonian, allowing the fluids from deeper formations to reach shallow surface through faults and fractures (e.g., Oliver, 1986; Mark et al., 2007). After that dissolution phase took place widening those fractures and forming vugs, which later were completely or partially sealed by calcite cement showing at least two generations of spar. This likely happened during Carboniferous-Permian rifting and magmatism, because the inclusions within the cements show two homogenization temperature peaks at 90–100 and 120–140 °C, that could be explained by the magmatic intrusions and the associated hydrothermal fluid flows in the area (e.g., Šliaupa and Hoth, 2011; Motuza et al., 2015). The two temperature intervals may be reflected by the two generations of cement. $\delta^{13}C$ and $\delta^{18}O$ of calcite within the veins and vugs are clustered around −0.8‰–1.8‰ for $\delta^{13}C$ and −6‰ to −2‰ for $\delta^{18}O$, suggesting

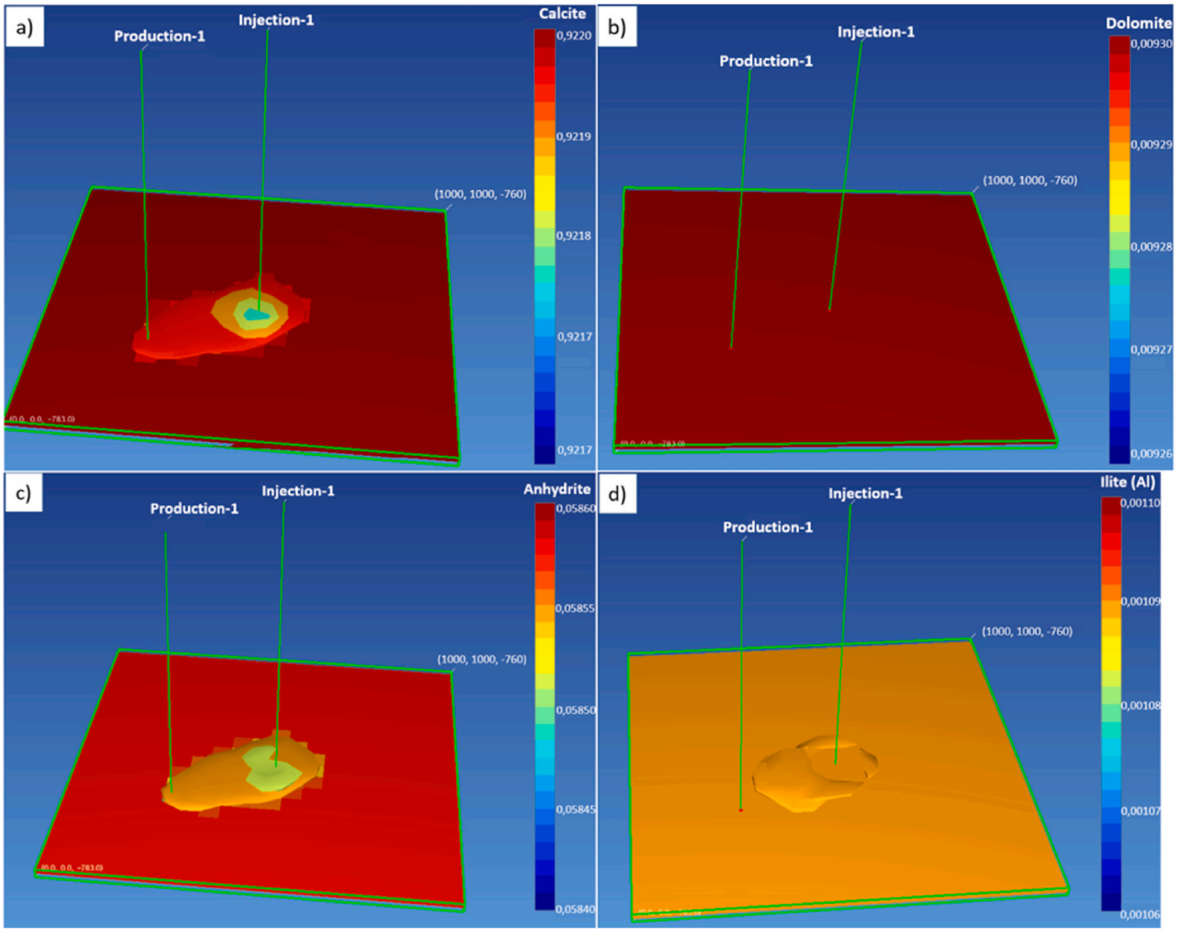

Fig. 16. Spatial a) calcite, b) dolomite, c) anhydrite, and d) illite variation between injection and production wells in the calcite-rich Pavasaris reef after 15 years of water-rock interaction simulations.

that meteoric water could have infiltrated the system due to re-activation of faults and was heated by the magmatic activities in the area (e.g., Allan and Matthews, 1990; Buschaert et al., 2004; Swart and Oehlert, 2018).

Values of $\delta^{13}C$ and $\delta^{18}O$ of dolomitized samples taken from several different reef structures and wells show correlation, suggesting that the source of dolomitizing fluids and the time of dolomitization is similar to all studied reef structures. The dolomitized porous sections of reservoirs typically have oil stains suggesting that dolomitization occurred prior to oil inflow into the system. The origin of the dolomitizing fluids is associated with water squeezed from clay, which is enriched with Fe and Mg cations. Therefore, dolomitization may have happened during the rapid burial in the Triassic, when underlaying and adjacent shales or clay within the Silurian formation underwent compaction (Stentoft et al., 2003). Following the dolomitization, being buried to sufficient depths for chemical compaction, stylolites were formed as well as the small tension gashes associated to stylolites.

Since the density of dolomite is higher than that of calcite, secondary pores were formed during the dolomitization and some calcite was redistributed within the system. Stylolite surfaces and the enlarged pores then acted as pathways for fluid flow, allowing for pyrite and silica precipitation, likely contemporaneously with the calcite and dolomite cementation. Then, leaching progressed, during which stylolites, tension gashes as well as intra- and intergranular pores were solution-enlarged. Lastly, the oil has accumulated within the rock.

Inclusion data thus show that the largest porosity losses of the Silurian carbonates are associated with the two largest thermal events that have taken place during the Late Silurian-Devonian continent-continent collision as well as the Carboniferous-Permian rifting and magmatism, that created suitable conditions for cementation. The results are in opposition to Bičkauskas (2017) study that concluded that the system is closed due to low porosity and permeability of the overlaying and underlaying rocks dominated by fine-grained carbonate mud, suggesting that diagenesis must have been driven by the original mineralogical composition of the sediment in combination with increasing effective pressure and temperature as a result of burial. However, knowing that currently the rocks are buried to their maximum depth (*c.*800 m), burial alone could not explain the paleotemperatures retrieved by inclusion tests performed in this study and chitinozoan reflectivity measurements done by Lazauskiene and Marschall (2002). Therefore, the system should have been open, most likely allowing fluids to come up from deeper layers through fractures and faults.

7.2. CO_2-water-rock interaction processes within Silurian reefs

3D simulation results show that the dissolution of dolomite and calcite are the dominant reactions during the whole process of CO_2-water-carbonate interactions for all cases. In the studied reef intervals, at the current state the formation water is close to equilibrium with carbonate minerals. However, 3D CO_2-water-rock interaction simulation shows that in the calcite-rich reef intervals, Ca^{2+} increases slowly at the very beginning of the simulation and starts to decline after about 0.5 years. Similarly, Mg^{2+} also increases slowly in the early stage, but the increase accelerates after 0.1 years. Calcite dissolution is generally dependent on temperature and acidity of the solution. A decrease in temperature and pH generally leads to an enhanced dissolution of

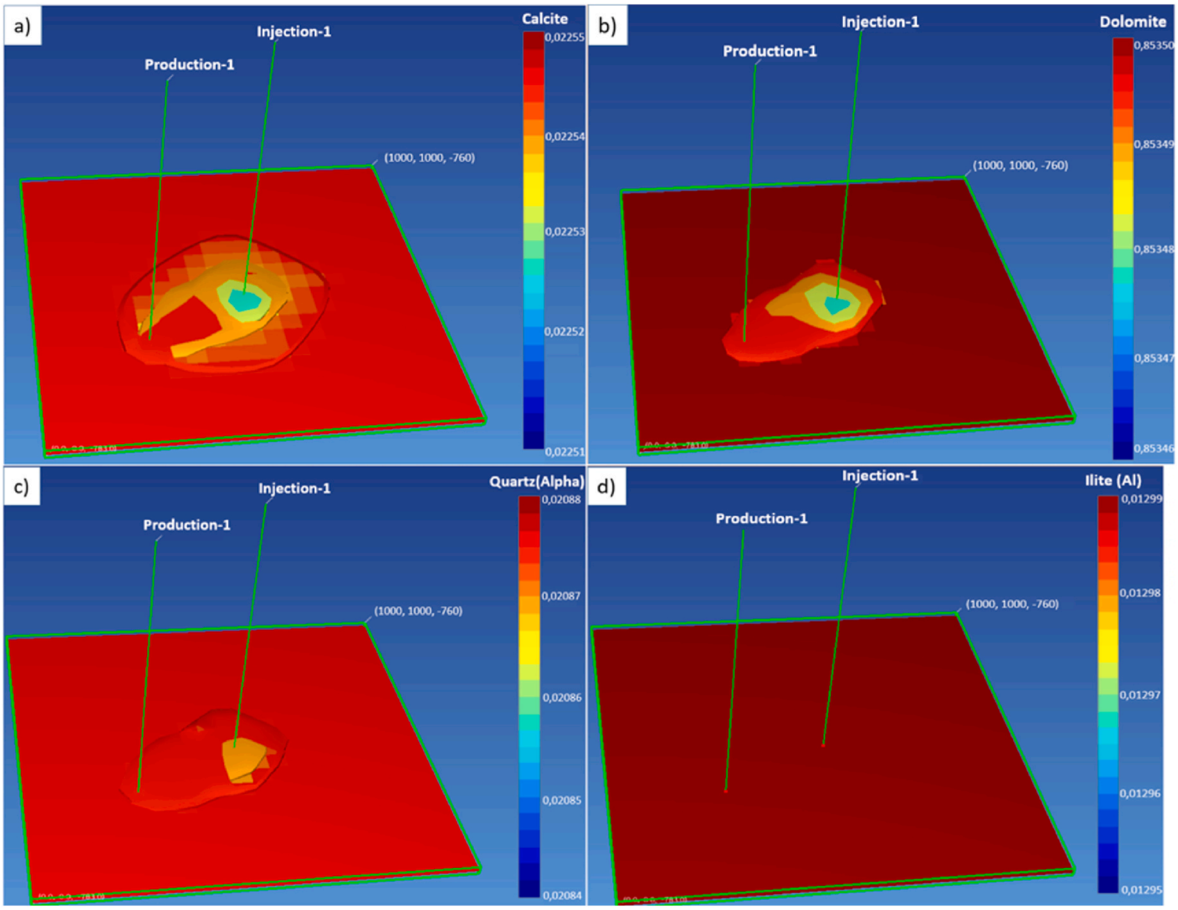

Fig. 17. Spatial a) calcite, b) dolomite, c) anhydrite, and d) illite variation between injection and production wells in the dolomitized Kudirka reef interval after 15 years of water-rock interaction simulations.

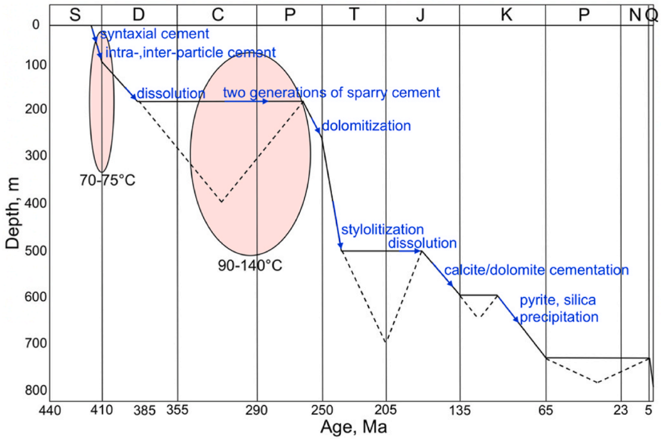

Fig. 18. Burial history diagram of the Silurian reefal deposits in Lithuania (modified from Stentoft et al., 2003). Thermal events are shown in red, and the likely hydrothermal deformation processes are marked in blue. (For interpretation of the references to colour in this figure legend, the reader is referred to the Web version of this article.)

calcite. Dolomite also shows temperature-dependent solubility, but its behaviour can be more complex due to its dual cation composition (calcium and magnesium). Like calcite, dolomite solubility in pure water decreases as temperature increases. This phenomenon was observed in the present study, where a decline in the injection well's temperature coincided with a decrease in pH. This combined effect resulted in the dissolution of dolomite and calcite minerals, evident from the observed decrease in their volume fraction and the corresponding rise in the concentration of Ca^{2+} and Mg^{2+} ions. This had a positive effect on porosity, because in all cases, porosity of the reservoir rocks increased over the 15-year injection period (Fig. 19). The lowest porosity increase is observed for the dolomitized reef interval, because dolomite dissolution is slower compared to calcite at the decreasing temperature.

Iron is found in many forms within the reefs but mostly as pyrite and siderite grains within the micrite matrix or as single crystals or aggregates within the cement on the fracture surface. However, overal the iron content within the rock is no more than 1–3 %. Based on 2D geochemical water modelling analysis, both at current reservoir temperature, and at cooling down of water to 10 °C, small amounts of hematite, goethite, Fe-rich talc and siderite are likely to precipitate in all of the studied reef structures and associated heat pumps and well infrastructure. The largest undersaturation in all the wells is typical for Fe-sulphides (pyrite FeS2, mackinawite FeS, FeSppt) that are likely to dissolve at both conditions. However, based on 3D CO_2-water-rock interaction simulation results, iron volume changes are insignificant, and it shouldn't have any effect on porosity changes.

Carbonate reservoirs are heterogeneous systems with anisotropic characteristics. To examine the effects of permeability variation on the reaction between injected brine and reservoir rock, we increased the permeability of grid blocks along the production and injection wells using a permeability factor (Fig. 20). The permeability of the highlighted grid blocks was doubled. We increased injection and production rates similarly from 5 to 10 kg/s.

It was found that increasing the permeability of grid blocks and the injection rate did not change the trend behaviour of porosity change, but

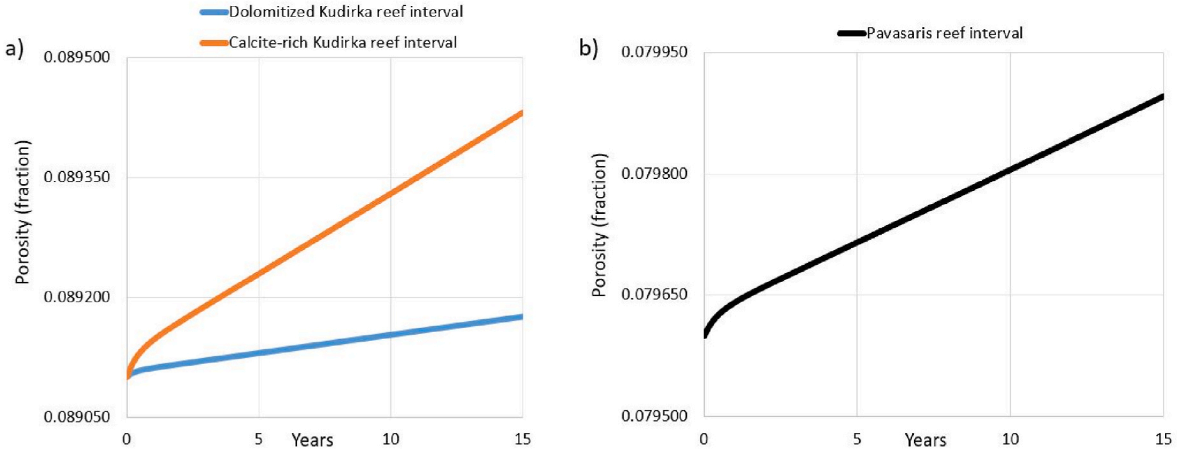

Fig. 19. Porosity (fraction) changes in the a) Kudirka, and b) Pavasaris reefs based on 15 years of CO_2-water-rock interaction simulations.

Fig. 20. Permeability variation along the grid blocks.

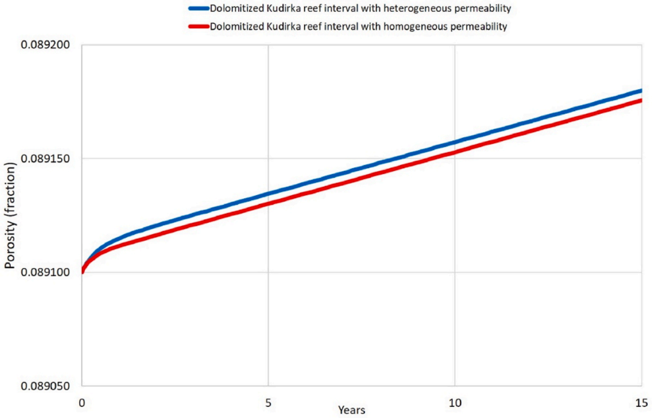

Fig. 21. Comparison of porosity changes with increased heterogeneity of the dolomitized Kudirka Reef interval.

the magnitude of porosity enhancement improved by a fraction of 0.0002 (Fig. 21). This is possibly related to the increase in the amount of dissolved minerals due to the higher injection rate achieved through increased permeability.

Keeping CO_2 in solution allows pressure control which is an effective method in maintaining mineral solubility to avoid carbonate scaling (Luo et al., 2023, and references therein). Additional injection of CO_2 also shifts the chemical equilibrium of carbonate. Adding CO_2 or other acid (e.g., HCl) lowers the pH level of water, that increases carbonate dissolution in the rock. The main disadvantage of HCl is that it is hazardous and using it will cause increase in the salinity of the groundwater (Kallesøe et al., 2019). Adding inhibitors can further increase the degree of oversaturation that is possible without precipitation (Finster et al., 2015).

8. Conclusions

With over 70 exploratory wells drilled through Silurian carbonate formations that are currently indicated as abandoned, plugged, buried and/or inactive, Silurian reef structures in the Middle Lithuania provide potential reservoirs for low enthalpy geothermal heat exploration. Temperature of the reefal reservoirs is around 32 °C. Kudirka and Pavasaris reef structures could provide enough thermal energy to the surrounding towns during the heating season. The water of the Silurian formation is of the chloride-calcium type with total mineralization between 74.1 and 106.2 g/l and pH between 6.4 and 6.7. Low reservoir temperatures and even lower injection temperatures provide good conditions for the sustainable heat extraction for a continuous 15-year period because porosity is maintained through dissolution that overwhelms the precipitation of carbonate minerals. A decrease in pH also leads to an enhanced dissolution of calcite, and in the current study a decline in the injection well's temperature coincided with a decrease in pH. This combined effect resulted in the dissolution of dolomite and calcite minerals, evident from the observed decrease in their volume fraction and the corresponding rise in the concentration of Ca^{2+} and Mg^{2+} ions. Studied cores from the wells also support simulation results, because they show several stages of dissolution. Vugs, solution enlarged fractures and stylolitic surfaces contain hydrothermal flow products such as calcite and dolomite cement, as well as grain replacing pyrite and quartz. The late-stage oil stains are also found within the vugs, fractures and stylolites, suggesting they acted as conduits to fluid flow. The largest porosity losses of the Silurian reefs are associated with the two largest thermal events that have taken place during the Late Silurian-Devonian continent-continent collision as well as the Carboniferous-Permian rifting and magmatism, that created suitable conditions for cementation. Primary inter- and intraparticle pores were largely filled by calcite cement, and the faults and fractures were at least partially filled by sparry calcite cement. Those large-scale calcite precipitation events are associated with high temperatures (70–140 °C) that wouldn't be reached during the geothermal heat extraction from these reservoirs. Simulation results show that dissolution is a more likely deformation process than the precipitation with a cold water injection and maximum temperature of the geothermal system reaching only up to 32 °C.

CRediT authorship contribution statement

Ieva Kaminskaite-Baranauskiene: Writing – review & editing, Writing – original draft, Visualization, Validation, Supervision, Software, Resources, Project administration, Methodology, Investigation, Funding acquisition, Formal analysis, Data curation, Conceptualization. **Hakki Aydin:** Writing – review & editing, Writing – original draft, Visualization, Methodology, Formal analysis, Data curation. **Zhida Liu:** Writing – review & editing, Writing – original draft, Visualization, Methodology, Formal analysis, Data curation.

Declaration of competing interest

The authors declare the following financial interests/personal relationships which may be considered as potential competing interests: Ieva Kaminskaite-Baranauskiene reports financial support was provided by Research Council of Lithuania. If there are other authors, they declare that they have no known competing financial interests or personal relationships that could have appeared to influence the work reported in this paper.

Acknowledgements

This project has received funding from the Research Council of Lithuania (LMTLT), agreement No S-MIP-22-49. The authors would like to thank Dr Anna Cichon Pupienis for providing critical review and valuable input to the discussion of the results. Thanks also go to the editor in chief and two anonymous reviewers for their insight and comments that improved the manuscript.

Data availability

No data was used for the research described in the article.

References

Allan, J.R., Matthews, R.K., 1990. Isotope signatures associated with early meteoric diagenesis. Carbonate Diagenesis, pp. 197–217.

Andre, B.J., Rajaram, H., 2005. Dissolution of limestone fractures by cooling waters: Early development of hypogene karst systems. Water Resources Research 41 (1).

Bičkauskas, G., 2017. Sedimentology and Diagenesis of Minija Regional Stage (Silurian) Carbonates in Lithuania. Vilniaus universitetas (Doctoral dissertation.

Biehl, B.C., Reuning, L., Schoenherr, J., Lüders, V., Kukla, P.A., 2016. Impacts of hydrothermal dolomitization and thermochemical sulfate reduction on secondary porosity creation in deeply buried carbonates: a case study from the Lower Saxony Basin, northwest Germany. AAPG (Am. Assoc. Pet. Geol.) Bull. 100 (4), 597–621.

Biot, M.A., 1956. Theory of propagation of elastic waves in a fluid-saturated porous solid. II. Higher frequency range. The Journal of the acoustical Society of america 28 (2), 179–191.

Bodnar, R.J., 1993. Revised equation and table for determining the freezing point depression of H2O–NaCl solutions. Geochem. Cosmochim. Acta 57 (1993), 683–684.

Buschaert, S., Fourcade, S., Cathelineau, M., Deloule, E., Martineau, F., Ougougdal, M.A., Trouiller, A., 2004. Widespread cementation induced by inflow of continental water in the eastern part of the Paris basin: O and C isotopic study of carbonate cements. Appl. Geochem. 19 (8), 1201–1215.

Cheng, Y., Fu, L.Y., Hou, W., Carcione, J.M., Deng, W., Wang, Z., 2024. Thermo-poroelastic AVO modeling of Olkaria geothermal reservoirs. Geoenergy Science and Engineering 241, 213166.

Cicha-Szot, R., Budak, P., 2016a. Special analysis of cores from Tidikas-1 well with interpretation. Oil and Gas Institute – National Research Institute (Industry report No. DK-4100-217/15). Industry report of UAB "TAN OIL". Retrieved from Lithuanian Geological Survey archive: unpublished.

Cicha-Szot, R., Budak, P., 2016b. Special analysis of cores from Bedugnis-1 well with interpretation. Oil and Gas Institute – National Research Institute. Industry report of UAB "TAN OIL". Retrieved from Lithuanian Geological Survey archive: unpublished.

Davies, G.R., Smith Jr, L.B., 2006. Structurally controlled hydrothermal dolomite reservoir facies: an overview. AAPG Bull. 90 (11), 1641–1690.

Finster, M., Clark, C., Schroeder, J., Martino, L., 2015. Geothermal produced fluids: characteristics, treatment technologies, and management options. Renew. Sustain. Energy Rev. 50, 952–966.

Garrison, R.E., 1981. Diagenesis of Oceanic Carbonate Sediments: a Review of the DSDP Perspective.

Hou, W., Fu, L.Y., Carcione, J.M., 2022. Reflection and transmission of thermoelastic waves in multilayered media. Geophysics 87 (3), MR117–MR128.

Jiang, Y., Gu, Y., Zhu, X., Xu, W., Xiao, Y., Li, J., 2017. Hydrothermal dolomite reservoir facies in the sinian dengying Fm, central sichuan basin. Nat. Gas. Ind. B 4 (4), 287–293.

Jiang, L., Pan, W., Cai, C., Jia, L., Pan, L., Wang, T., Li, H., Chen, S., Chen, Y., 2015. Fluid mixing induced by hydrothermal activity in the ordovician carbonates in Tarim Basin, China. Geofluids 15 (3), 483–498.

Jiu, B., Huang, W., Mu, N., He, M., 2020. Effect of hydrothermal fluids on the ultra-deep Ordovician carbonate rocks in Tarim Basin, China. J. Petrol. Sci. Eng., 107445

Kallesøe, A.J., Vangkilde-Pedersen, T., Nielsen, J.E., Bakema, G., Egermann, P., Hahn, F., 2019. HEATSTORE–Underground thermal energy storage (UTES)-State of the art. In: Example cases and lessons learned, p. 1.

Kaminskaite-Baranauskiene, I., Cichon-Pupienis, A., Makauskas, P., 2024. Silurian barrier reef in Lithuania: reservoir properties and low enthalpy geothermal heat potential. Heliyon, e26360. https://doi.org/10.1016/j.heliyon.2024.e26360.

Lazauskiene, J., Marschall, J., 2002. Chitinozoan reflectance and the thermal history of the lower palaeozoic sediments of the Baltic basin. In: 5th Baltic Stratigraphic Conference, pp. 93–97. Vilnius.

Ledésert, B., Hebert, R., Genter, A., Bartier, D., Clauer, N., Grall, C., 2010. Fractures, hydrothermal alterations and permeability in the soultz enhanced geothermal system. Compt. Rendus Geosci. 342 (7–8), 607–615.

Li, N., Deng, W., Fu, L.Y., Carcione, J.M., Han, T., 2022. Wave propagation in double-porosity thermoelastic media. Geophysics 87 (6), MR265–MR277. https://doi.org/10.1190/geo2022-0008.1.

Li, N., Fu, L.Y., Deng, W., Carcione, J.M., Yang, J., 2023. A thermo-hydro-mechanical model to evaluate the seismic properties of geothermal reservoirs. Geophysics 88 (5), WB23–WB35.

Li, H., Jin, F., Xiao, D., Pu, X., Jiang, W., 2021. Provenance and sedimentary environment of the Ek2 shale in the cangdong sag, the central bohai bay basin, China. Interpretation 9, T1139–T1156.

Li, H., Liu, B., Liu, X., Meng, L., Cheng, L., Wang, H., 2019. Mineralogy and inorganic geochemistry of the Es4 shales of the damintun sag, northeast of the bohai bay basin: implication for depositional environment. Mar. Petrol. Geol. 110, 886–900.

Luo, W., Kottsova, A., Vardon, P.J., Dieudonné, A.C., Brehme, M., 2023. Mechanisms causing injectivity decline and enhancement in geothermal projects. Renew. Sustain. Energy Rev. 185, 113623.

Mansurbeg, H., Morad, D., Othman, R., Morad, S., Ceriani, A., Al-Aasm, I., Kolo, K., Spirov, P., Proust, J.N., Preat, A., Koyi, H., 2016. Hydrothermal dolomitization of the bekhme formation (upper cretaceous), zagros basin, kurdistan region of Iraq: record of oil migration and degradation. Sediment. Geol. 341, 147–162.

Mark, D.F., Parnell, J., Kelley, S.P., Sherlock, S.C., 2007. Resolution of regional fluid flow related to successive orogenic events on the Laurentian margin. Geology 35 (6), 547–550.

Matyasik, I., Lesniak, G., 2016. Oil and reservoir water analyses from Vilkaviskis-135 well with interpretation. Oil and Gas Institute – National Research Institute (Industry report No. DK-4100-212/16). Industry report of UAB "Diseta". Retrieved from Lithuanian Geological Survey archive: unpublished.

Menezes, C.P., Bezerra, F.H., Balsamo, F., Mozafari, M., Vieira, M.M., Srivastava, N.K., de Castro, D.L., 2019. Hydrothermal silicification along faults affecting carbonate-sandstone units and its impact on reservoir quality, Potiguar Basin, Brazil. Mar. Petrol. Geol. 110, 198–217.

Micklethwaite, S., Cox, S.F., 2004. Fault-segment rupture, aftershock-zone fluid flow, and mineralization. Geology 32 (9), 813–816.

Motuza, G., Šliaupa, S., Timmerman, M.J., 2015. Geochemistry and 40 Ar/39 Ar age of early carboniferous dolerite sills in the southern baltic sea. Est. J. Earth Sci. 64 (3).

Oliver, J., 1986. Fluids expelled tectonically from orogenic belts: their role in hydrocarbon migration and other geologic phenomena. Geology 14 (2), 99–102.

Palandri, J., Kharaka, Y.K., 2004. A compilation of rate parameters of water– mineral interaction kinetics for application to geochemical modeling. US Geological Survey Open File Report 2004-1068 64.

Sigfússon, B., Uihlein, A., 2015. 2014 JRC geothermal energy status report. .

Stentoft, N., Lapinskas, P., Musteikis, P., 2003. Diagenesis of Silurian reefal carbonates, Kudirka oilfield, Lithuania. J. Petrol. Geol. 26 (4), 381–402.

Su, Y., Yang, F., Wang, B., Jia, Z., Duan, Z., 2018. Reinjection of cooled water into sandstone geothermal reservoirs in China: a review. Geosciences Journal 22, 199–207.

Swart, P.K., Oehlert, A.M., 2018. Revised interpretations of stable C and O patterns in carbonate rocks resulting from meteoric diagenesis. Sediment. Geol. 364, 14–23.

Šliaupa, S., Hoth, P., 2011. Geological evolution and resources of the baltic sea area from the precambrian to the quaternary. The Baltic Sea Basin 13–51.

Wagner, R., Kühn, M., Meyn, V., Pape, H., Vath, U., Clauser, C., 2005. Numerical simulation of pore space clogging in geothermal reservoirs by precipitation of anhydrite. International Journal of Rock Mechanics and Mining Sciences 42 (7–8), 1070–1081.

Xu, T., Sonnenthal, E., Spycher, N., Pruess, K., 2006. TOUGHREACT a simulation program for non-isothermal multiphase reactive geochemical transport in variably saturated geologic media: applications to geothermal injectivity and CO2 geological sequestration. Comput. Geosci. 32 (2), 145–165.

Zdanavičiūtė, O., Jacyna, J., 2003. Mokslinio tyrimo darbo "Silūro rifų paplitimo dėsningumų ir jų naftos perspektyvų įvertinimas bei pasiūlymų tolimesniems naftos darbams vykdyti pateikimas". Industrial report of UAB „Minijos nafta", Geology and geography institute 2600, 13. Vilnius.

Zhu, D., Jin, Z., Hu, W., 2010. Hydrothermal recrystallization of the Lower Ordovician dolomite and its significance to reservoir in northern Tarim Basin. Sci. China Earth Sci. 53 (3), 368–381.